(12) INTERNATIONAL APPLICATION PUBLISHED UNDER THE PATENT COOPERATION TREATY (PCT)

(19) World Intellectual Property Organization
International Bureau

(43) International Publication Date
9 February 2012 (09.02.2012)

PCT

(10) International Publication Number
WO 2012/018777 A1

(51) International Patent Classification:
B82Y 15/00 (2011.01) *A61B 5/145* (2006.01)
B82Y 30/00 (2011.01) *G01N 33/487* (2006.01)

(21) International Application Number:
PCT/US2011/046214

(22) International Filing Date:
2 August 2011 (02.08.2011)

(25) Filing Language: English

(26) Publication Language: English

(30) Priority Data:
61/400,807 3 August 2010 (03.08.2010) US

(71) Applicant *(for all designated States except US)*: **UNIVERSITY OF CONNECTICUT** [US/US]; 263 Farmington Avenue, Farmington, CT 06030-6400 (US).

(72) Inventors; and

(75) Inventors/Applicants *(for US only)*: **LEI, Yu** [CN/US]; 46 Adeline Place, Mansfield Center, CT 06250 (US). **DING, Yu** [CN/CN]; Lane 123, Guiping Road, Shanghai, 200233 (CN).

(74) Agent: **LONG, Timothy, M.**; McDonnell Boehnen Hulbert & Berghoff LLP, 300 South Wacker Drive, Suite 3100, Chicago, IL 60606 (US).

(81) Designated States *(unless otherwise indicated, for every kind of national protection available)*: AE, AG, AL, AM, AO, AT, AU, AZ, BA, BB, BG, BH, BR, BW, BY, BZ, CA, CH, CL, CN, CO, CR, CU, CZ, DE, DK, DM, DO, DZ, EC, EE, EG, ES, FI, GB, GD, GE, GH, GM, GT, HN, HR, HU, ID, IL, IN, IS, JP, KE, KG, KM, KN, KP, KR, KZ, LA, LC, LK, LR, LS, LT, LU, LY, MA, MD, ME, MG, MK, MN, MW, MX, MY, MZ, NA, NG, NI, NO, NZ, OM, PE, PG, PH, PL, PT, RO, RS, RU, SC, SD, SE, SG, SK, SL, SM, ST, SV, SY, TH, TJ, TM, TN, TR, TT, TZ, UA, UG, US, UZ, VC, VN, ZA, ZM, ZW.

(84) Designated States *(unless otherwise indicated, for every kind of regional protection available)*: ARIPO (BW, GH, GM, KE, LR, LS, MW, MZ, NA, SD, SL, SZ, TZ, UG, ZM, ZW), Eurasian (AM, AZ, BY, KG, KZ, MD, RU, TJ, TM), European (AL, AT, BE, BG, CH, CY, CZ, DE, DK, EE, ES, FI, FR, GB, GR, HR, HU, IE, IS, IT, LT, LU, LV, MC, MK, MT, NL, NO, PL, PT, RO, RS, SE, SI, SK, SM, TR), OAPI (BF, BJ, CF, CG, CI, CM, GA, GN, GQ, GW, ML, MR, NE, SN, TD, TG).

[Continued on next page]

(54) Title: NON-ENZYMATIC GLUCOSE SENSORS BASED ON METAL OXIDE NANOMATERIALS

(57) Abstract: Non-enzymatic glucose sensors are described based on optionally metal-doped metal oxide nanofibers for glucose detection in alkaline solution (e.g., pH 13). Such sensors can show a fast response time, a high sensitivity, good reproducibility and selectivity, and a good detection limit. Unlike precious metal based non-enzymatic glucose sensors, the sensors herein are not poisoned by high concentrations of NaCl, are not affected by oxygen, and remain electrocatalytically active in alkaline solutions above 40 °C.

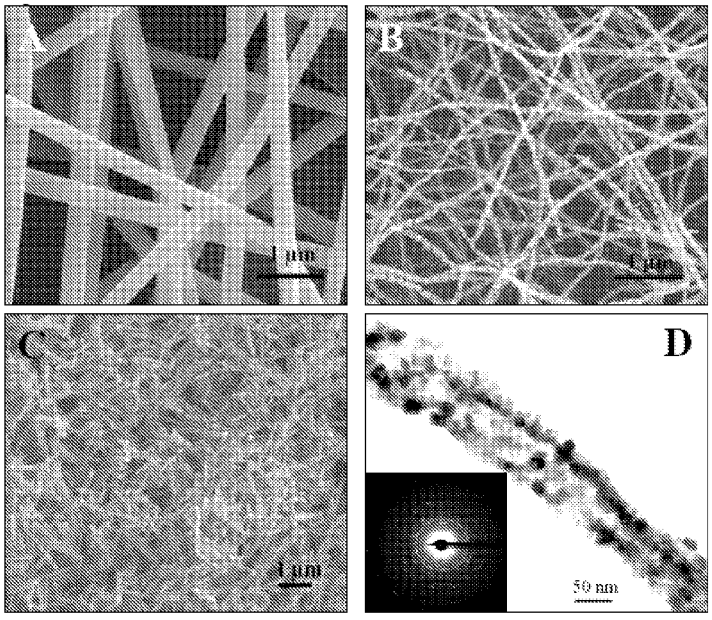

Figure 1

WO 2012/018777 A1

Published:

— *with international search report (Art. 21(3))*

NON-ENZYMATIC GLUCOSE SENSORS BASED ON METAL OXIDE NANOMATERIALS

CROSS-REFERENCE TO RELATED APPLICATIONS

This application claims the benefit of the filing date of U.S. Provisional Application Serial No. 61/400,807, filed August 3, 2010, which is hereby incorporated by reference in its entirety.

STATEMENT OF GOVERNMENT INTEREST

The invention described herein was made in part with government support under grant number CMMI 0730826 awarded by the National Science Foundation; and grant number DE-FE0000870, awarded by the Department of Energy. The United States Government has certain rights in the invention.

FIELD OF THE INVENTION

The present invention is in the field of sensors for blood glucose monitoring and, more specifically, for non-enzymatic glucose sensors.

BACKGROUND OF THE INVENTION

Glucose detection has various applications ranging from clinical diagnosis of diabetes to fermentation and food quality control. Glucose sensors can be generally classified into two categories: glucose oxidase (GOx) based sensors and non-enzymatic glucose sensors. In GOx-based sensors, oxygen is reduced by GOx to H_2O_2 while glucose is oxidized to gluconolactone. Thus, glucose detection by GOx-based sensors normally depends on the response from H_2O_2 oxidation or oxygen reduction. Owing to the high selectivity and fast response of the enzymatic reaction, GOx-based sensors have been widely studied. However, due to the intrinsic feature of enzymes, GOx-based biosensors suffer from stability problems. In addition, GOx-based test strips are not cost-effective for use in developing countries due the cost of the enzyme.

Therefore, it is important to develop cheap, sensitive, and selective non-enzymatic sensors for glucose detection. A variety of transition metals (e.g. Au, Cu, Pt, Ni) and metal oxides (e.g. CuO, NiO, cobalt oxide) have been explored to construct enzyme-free glucose sensors. (See, e.g., Li et al., *Electrochem. Commun.*, 2007, **9**, 981-988; Nagy, L. et al., *Sens. Actuators, B*, 2001, **76**, 494-499; Park, S. et al., *Anal. Chem.*, 2003, **75**, 3046-3049; You, T.Y. et al., *Anal. Chem.*, 2003, **75**, 5191-5196; Lu, L.M. et al., *Biosens. Bioelectron.*, 2009, **25**, 218-223; Reitz, E. et al., *Electroanalysis*, 2008, **20**, 2482-2486; Cheng, X. et al., *Food Chem.*,

2008, **106**, 830-835; and Casella, I.G., *J. Electroanal. Chem.*, 2002, **520**, 119-125). Additionally, carbon nanotubes (CNTs) have also been reported for glucose electrooxidation. In order to further improve the performance of the non-enzymatic glucose sensors, different alloys (e.g. Pt-Pb, Ni-Cu, Au-Ag) and metals or metal oxides-CNTs composites (e.g. Au nanoparticles-MWNTs, Cu_2O-MWNTs nanocomposites, and MnO_2-MWNTs) have been proposed. (See, e.g., Sun, Y. P. et al., *Anal. Chem.*, 2001, **73**, 1599-1604; Yeo and Johnson, *J. Electroanal. Chem.*, 2001, **495**, 110-119; Tominaga, M. et al., *J. Electroanal. Chem.*, 2006, **590**, 37-46; Zhu, H. Et al., *Talanta*, 2009, **79**, 1446-1453; Zhang, X. J. et al., *Biosens. Bioelectron.*, 2009, **24**, 3395-3398; and Chen, J. et al., *Electrochem. Commun.*, 2008, **10**, 1268-1271). However, non-enzymatic glucose sensors often lack good selectivity, which can greatly limit their clinical application.

SUMMARY OF THE INVENTION

As described herein, metal oxide nanofibers and metal-doped metal oxide nanofibers (e.g. Co_3O_4, NiO, and/or CuO nanofibers) can be prepared by, for example, electrospinning and subsequent calcination. The as-prepared nanofibers can be applied to construct a non-enzymatic sensor for glucose detection in alkaline solution (e.g., pH 13). Such sensors can show a fast response time (less than 7 s), high sensitivity, and good reproducibility, selectivity, and detection limit. Unlike precious metal based non-enzymatic glucose sensors, the sensors herein are not poisoned by high concentrations of NaCl, are not affected by oxygen, and remain electrocatalytically active in alkaline solutions above 40 °C.

Accordingly, in one aspect, the present disclosure provides non-enzymatic glucose sensors comprising an electrode, one or more metal oxide nanofibers, and an alkaline solid electrolyte, wherein the metal oxide nanofibers and an alkaline solid electrolyte are each disposed over a surface of the electrode, at least a portion of the alkaline solid electrolyte is in contact with the metal oxide nanofibers, and the metal oxide nanofibers are each independently and optionally metal doped.

In another aspect, the present disclosure provides glucose detection apparatuses comprising a non-enzymatic glucose sensor of the preceding aspect.

In another aspect, the present disclosure provides methods for preparing non-enzymatic glucose sensors comprising, depositing one or more metal oxide nanofibers and an alkaline solid electrolyte on an electrode surface, wherein the metal oxide nanofibers are optionally metal doped.

In another aspect, the present disclosure provides glucose test strips comprising a support material comprising a working electrode wherein the working electrode comprises a surface coating comprising one or more metal oxide nanofibers and an alkaline solid electrolyte, and wherein the metal oxide nanofibers are optionally metal-doped.

The sensors of the present invention, when applied for the detection of glucose in human blood serum, advantageously show excellent agreement with the results obtained from a commercial glucose meter (e.g., OneTouch UltraMini, LifeScan, Inc, CA). Further, the sensors herein have excellent selectivity against uric acid and ascorbic acid. Without being limited by any one theory of operation, under alkaline condition (e.g., pH 13), the metal oxide surfaces would be negatively charged resulting in a "repelling effect". Under the same conditions, potentially interfering compounds, such as uric acid (UA) and ascorbic acid (AA), would also be negatively charged due to the loss of proton. Consequently, the negatively charged metal oxide surface could strongly repel the negatively charged UA and AA molecules, thus greatly reducing the electrooxidation of UA and AA on the surface of metal oxides and resulting in good selectivity.

The non-enzymatic glucose sensors described herein have great commercial potential in clinical diagnosis of diabetes due to their excellent performance, good reproducibility, low cost, and inherent stability of the component inorganic materials.

BRIEF DESCRIPTION OF THE DRAWINGS

Figure 1 shows (A) SEM image of polyvinylpyrrolidone(PVP)/$Co(NO_3)_2$ nanofibers; (B) Co_3O_4 nanofibers (C) Co_3O_4 nanofibers after 1 h sonication in ethanol; and (D) TEM image of a single Co_3O_4 nanofiber (inset: SAED patterns of Co_3O_4 nanofibers).

Figure 2 shows (A) FTIR spectra of PVP/$Co(NO_3)_2$ nanofibers (a) and Co_3O_4 nanofibers (b); and (B) Raman spectra of PVP/$Co(NO_3)_2$ nanofibers (a) and Co_3O_4 nanofibers (b).

Figure 3 shows (A) XRD patterns for the standard values of JCPDS 42-1467 (a), and the as-prepared Co_3O_4 nanofibers (b); and (B) a high resolution X-Ray photoelectron spectrum for Co 2p regions of the Co_3O_4 nanofibers.

Figure 4a shows cyclic voltammograms (CVs) of the Co_3O_4 nanofibers (NFs)-Nafion/GCE in 0.1 M pH 7 phosphate buffer solution (a) and 0.1 M NaOH solution (b) at a scan rate of 100 mV/s.

Figure 4b shows CVs of the Co_3O_4 NFs-Nafion/glassy carbon electrode(GCE) in 0.1 M NaOH solution at various scan rates of 25, 50, 75, 100, 125, 150, 175, 200 mV/s.

Figure 4c shows a plot of peak currents vs. scan rate for Co_3O_4 NFs-Nafion/glassy carbon electrode (GCE).

Figure 5a shows CVs of the Nafion/GCE (a and b) and Co_3O_4 NFs-Nafion/GCE (c and d) in 0.1 M NaOH in the absence (a and c) and presence (b and d) of 2.8 mM glucose, respectively.

Figure 5b shows the amperometric response of the Co_3O_4 NFs-Nafion/GCE with successive additions of glucose to 0.1 M NaOH at an applied potential of +0.59 V. Inset: the response of the Nafion/GCE as a control.

Figure 5c shows a corresponding calibration curve with fitting curve and linear range for the amperometric response of Figure 5b.

Figure 5d shows the amperometric response of Co_3O_4 NFs-Nafion/GCE with successive 3-time additions of analytes in the sequence of 5 μL blood serum sample, 5 μL 10 mM glucose in buffer, 10 μL blood serum sample, and 10 μL 10 mM glucose in buffer.

Figure 6 shows (A) a schematic illustration for the selective catalytic reaction towards glucose; (B) the response of Nafion modified bare GCE to the addition of 4 mM glucose (a), 0.125 mM ascorbic acid (AA) (b), 0.33 mM uric acid (UA) (c); (C) the response of the Co_3O_4 NFs-Nafion/GCE to the addition of 4 mM glucose (a), 4 mM glucose with 0.125 mM AA (b), 4 mM glucose with 0.33 mM UA (c), 0.125 mM AA (d), 0.33 mM UA (e) in 0.1 M NaOH.

Figure 7 shows SEM images of (a) $AgNO_3$-PVP nanofibers; (b) porous Ag obtained after calcination of $AgNO_3$-PVP nanofibers; (c) $Ni(NO_3)_2$-PVP nanofibers; (d) NiO nanofibers; (e) $Ni(NO_3)_2$-$AgNO_3$-PVP nanofibers; (f) NiO-Ag nanofibers.

Figure 8 shows TEM images of (a) a $Ni(NO_3)_2$-$AgNO_3$-PVP nanofiber; (b) a NiO nanofiber; (c) a NiO–Ag hybrid nanofiber; insets show the EDX mapping of Ag, Ni and O elements; (d) SAED pattern of NiO-Ag hybrid nanofiber; (e) EDX analysis of NiO-Ag hybrid nanofibers; inset: EDX analysis of $Ni(NO_3)_2$-$AgNO_3$-PVP nanofibers. C and Cu peaks come from the copper-carbon grid of TEM

Figure 9a shows FTIR spectra of $Ni(NO_3)_2$-$AgNO_3$-PVP nanofibers, porous Ag, NiO nanofibers and NiO-Ag nanofibers.

Figure 9b shows XRD patterns for the standard values of JCPDS 04-0835 (NiO, solid line) and 04-0783 (Ag, dash-dot line), and the as-prepared porous Ag, NiO nanofibers and NiO-Ag nanofibers.

Figure 9c shows high resolution X-Ray photoelectron spectra for Ni 2p region of the NiO-Ag nanofibers.

Figure 9d shows high resolution X-Ray photoelectron spectra for Ag 3d region of the NiO-Ag nanofibers.

Figure 10 shows CVs of (a) NiO NFs/GCE, (b) porous Ag/GCE, and (c)NiO-Ag NFs/GCE in 0.1 M NaOH in the absence (trace a) and presence of 8 mM glucose (trace b), respectively (Scan rates = 100 mV/s).

Figure 11 shows (a) CVs of the NiO-Ag NFs/GCE in 0.1 M NaOH solution at various scan rates (10, 20, 40, 60, 80, and 100 mV/s); (b) plot of peak currents vs. scan rate.

Figure 12a shows hydrodynamic voltammograms of 200 μM glucose at the porous Ag/GCE, NiO NFs/GCE and NiO-Ag NFs/GCE.

Figure 12b shows amperometric response of porous Ag/GCE and NiO-Ag NFs/GCE to successive additions of glucose at an applied potential of 0.1 V.

Figure 12c shows amperometric response of porous NiO NFs/GCE and NiO-Ag NFs/GCE to successive additions of glucose at an applied potential of 0.6 V.

Figure 12d shows a calibration curves corresponding to the amperometric response of Figure 12b and 12c.

Figure 13 shows (a) the response of the porous Ag/GCE and the NiO-Ag NFs/GCE to the addition of 4 mM glucose, 0.125 mM AA and 0.33 mM UA in 0.1 M NaOH at an applied potential of 0.1 V; and (b) the response of the NiO NFs/GCE and the NiO-Ag NFs/GCE to the addition of 4 mM glucose, 4 mM glucose with 0.125 mM AA, and 4 mM glucose with 0.33 mM UA in 0.1 M NaOH at an applied potential of 0.6 V.

Figure 14 is a schematic illustration for the selective catalytic reaction towards glucose.

Figure 15 shows the amperometric response of the NiO-Ag NFs/GCE at 0.6 V with successive additions of different analytes; the ratio of glucose to UA and AA in testing electrolyte solution is in the similar ratio level as that in the blood sample.

DETAILED DESCRIPTION OF THE INVENTION

The non-enzymatic glucose sensors herein comprise one or more metal oxide nanofibers, wherein the metal oxide nanofibers are optionally metal doped. Suitable metal oxides include, but are not limited to Co_3O_4, NiO, CuO, or a mixture thereof. Thus, in certain embodiments, the metal oxide nanofibers comprise Co_3O_4 or NiO. In other embodiments, the metal oxide nanofibers comprise Co_3O_4. In other embodiments, the metal oxide nanofibers comprise NiO. However, in certain embodiments, the metal oxide nanofibers are not CuO nanofibers.

In yet other embodiments, the metal oxide nanofibers comprise a mixture of two or more of metal oxides. In one embodiment, the two metal oxides are selected from the group consisting of Co_3O_4, NiO, CuO, ZnO, SnO_2, CeO_2, MnO_2, RuO_2, and CdO. In another example, the metal oxide nanofibers comprise a mixture of two or more of metal oxides, where one metal oxide is Co_3O_4, NiO, or CuO (e.g., Co_3O_4 or NiO), and the other metal oxide is ZnO, SnO_2, CeO_2, MnO_2, RuO_2, or CdO. In another example, the metal oxide nanofibers can comprise NiO and CdO (i.e., NiO-CdO nanofibers).

In other embodiments, the metal oxide nanofibers comprise a mixture of three or more metal oxides. In one embodiment, the three metal oxides are selected from the group consisting of Co_3O_4, NiO, CuO, ZnO, SnO_2, CeO_2, MnO_2, RuO_2, and CdO. In another example, the metal oxide nanofibers comprise a mixture of three or more of metal oxides, where two metal oxide are selected from Co_3O_4, NiO, and CuO (e.g., Co_3O_4 and NiO), and the remaining metal oxide is ZnO, SnO_2, CeO_2, MnO_2, RuO_2, or CdO. In another example, the metal oxide nanofibers comprise a mixture of three or more of metal oxides, where one metal oxide is Co_3O_4, NiO, or CuO (e.g., Co_3O_4 or NiO), and the other two metal oxides are selected from ZnO, SnO_2, CeO_2, MnO_2, RuO_2, and CdO. For example, the metal oxide nanofibers can comprise Co_3O_4, NiO, and CuO (e.g., Co_3O_4-NiO-CuO nanofibers).

The term "nanofiber" as used herein means fibers comprising the referenced materials which have an average diameter of less than about 1000 nm and are can be prepared by electrospinning according to methods familiar to those skilled in the art, or according to the methods described below. When nanofibers comprise two or more constituent components, each of the components are separated by a dash "-" (e.g., NiO-CdO nanofibers comprise both NiO and CdO within the nanofibers). Further, when the nanofibers contain two or more metal oxide constituents, the two metal oxide components can be present in the nanofibers in any suitable molar ratio (e.g., in a 1:1, 1:2, 1:5, 1:10, 1:15, 1:20, 1:25, 1:30, 1:35, 1:40, 1:45, 1:50, 1:55, 1:60, 1:65, 1:70, 1:75, 1:80, 1:85, 1:90, 1:95, or 1:100 molar ratio of the two metal oxide components). Accordingly, unless otherwise defined, nanofibers containing two or more metal oxide constituents include all suitable molar ratios of the referenced components. For example, when the nanofibers are NiO-CdO nanofibers, NiO and CdO can be present in the nanofibers in a molar ratio of 1:1, 1:2, 1:5, 1:10, 1:15, 1:20, 1:25, 1:30, 1:35, 1:40, 1:45, 1:50, 1:55, 1:60, 1:65, 1:70, 1:75, 1:80, 1:85, 1:90, 1:95, or 1:100 of either NiO to CdO or CdO to NiO.

Accordingly, in certain other embodiments, the nanofibers are metal doped metal oxide nanofibers. The term "metal doped" as used herein means that the nanofibers comprise

one or more elemental metal component in addition to the metal oxide component within the nanofibers (e.g., NiO-Ag nanofibers comprise both NiO and Ag within the nanofibers). Such elemental metal component can be identified, for example, by transmission electron microscopy (TEM). In certain embodiments, the metal-doped metal oxide nanofibers comprise discrete domains of the metal and the metal oxide. In certain embodiments, the metal doped metal oxide nanofibers can comprise a mixture of metal oxide nanoparticles and metal nanoparticles which may be homogeneously or heterogeneously dispersed throughout the nanofibers. In certain embodiments, the metal doped metal oxide nanofibers can comprise a heterogeneous mixture of metal oxide nanoparticles and metal nanoparticles. Such metal doped metal oxide nanofibers herein are also referred to as "hybrid nanofibers." When used, hybrid nanofibers comprise each of the referenced constituents (i.e., the two or more components, each separated by a dash "-"). When the nanofibers are metal-doped metal oxide nanofibers, the metal and metal oxide components can be present in the nanofibers in any suitable molar ratio (e.g., 1:1, 1:2, 1:5, 1:10, 1:15, 1:20, 1:25, 1:30, 1:35, 1:40, 1:45, 1:50, 1:55, 1:60, 1:65, 1:70, 1:75, 1:80, 1:85, 1:90, 1:95, or 1:100 molar ratio of metal to metal oxide), provided that the metal oxides maintain a suitable fiber structure (e.g., comprise 50 mol% or more of the nanofibers). Accordingly, unless otherwise defined, metal-doped metal oxide nanofibers include all suitable molar ratio of the referenced components as defined above. For example for Ag-NiO nanofibers, Ag and NiO can be present in the nanofibers in a molar ratio of 1:1, 1:2, 1:5, 1:10, 1:15, 1:20, 1:25, 1:30, 1:35, 1:40, 1:45, 1:50, 1:55, 1:60, 1:65, 1:70, 1:75, 1:80, 1:85, 1:90, 1:95, or 1:100 of Ag to NiO.

In another example, the metal oxide nanofibers can be doped with one or more noble metals. In other embodiments, the nanofibers are noble metal-doped metal oxide nanofibers. "Noble metals" as used herein refers to metals selected from the group consisting of ruthenium, rhodium, palladium, silver, osmium, iridium, platinum, gold, and mixtures thereof. In certain embodiments, noble metals are metals selected from the group consisting of palladium, silver, platinum, gold, and mixtures thereof. Thus, in certain embodiment, the nanofibers are Ag-doped metal oxide nanofibers; or Au-doped metal oxide nanofibers; or Pt-doped metal oxide nanofibers; or Pd-doped metal oxide nanofibers.

Examples of suitable metal oxide nanofibers include, but are not limited to metal-doped NiO nanofibers, metal-doped Co_3O_4 nanofibers, metal-doped CuO nanofibers, noble metal-doped NiO nanofibers, noble metal-doped Co_3O_4 nanofibers, and noble metal-doped CuO nanofibers. Particular examples of metal-doped metal oxide nanofibers include, but are

not limited to, NiO-Ag nanofibers, Co_3O_4-Ag nanofibers, and CuO-Ag nanofibers or a combination thereof.

In certain embodiments, the metal-doped metal oxide hybrid nanofibers can comprise two or more metal oxides and one or more metal (e.g., one or more noble metal). For example, the metal-doped metal oxide nanofibers comprise a mixture of two or more of metal oxides (e.g., two of Co_3O_4, NiO, CuO, ZnO, SnO_2, CeO_2, MnO_2, RuO_2, and CdO) and one or more noble metal, as defined above. For example, the metal-doped metal oxide nanofibers can comprise NiO, CdO, and Ag (i.e., Ag-NiO-CdO nanofibers). In other embodiments, the metal oxide nanofibers comprise a mixture of three or more metal oxides (e.g., three of Co_3O_4, NiO, CuO, ZnO, SnO_2, CeO_2, MnO_2, RuO_2, and CdO) and one or more noble metal, as defined above. For example, the metal-doped metal oxide nanofibers can comprise Co_3O_4, NiO, CuO, and Ag (e.g., Ag-Co_3O_4-NiO-CuO nanofibers). When the nanofibers are metal-doped metal oxide nanofibers comprising two or more metal oxide components and/or two or more metal components, the total moles of metal component(s) and the total moles of the metal oxide components can be present in the nanofibers in any suitable molar ratio (e.g., 1:1, 1:2, 1:5, 1:10, 1:15, 1:20, 1:25, 1:30, 1:35, 1:40, 1:45, 1:50, 1:55, 1:60, 1:65, 1:70, 1:75, 1:80, 1:85, 1:90, 1:95, or 1:100 molar ratio of total moles of metal to total moles of metal oxide), provided that the metal oxide components maintain a suitable fiber structure (e.g., the total metal oxide component comprise 50 mol% or more of the nanofibers). Accordingly, unless otherwise defined, metal-doped metal oxide nanofibers comprising two or more metal oxide components and/or two or more metal components include all suitable molar ratio of the referenced components as defined above. For example for Ag-NiO-Co_3O_4 nanofibers, the relevant ratio is the moles of Ag to the total moles of NiO and Co_3O_4, such that the molar ratio is Ag to [NiO+Co_3O_4]. Similarly for Ag-Au-NiO nanofibers, the relevant ratio is the total moles of Ag and Au to the moles of NiO, such that the molar ratio is [Ag + Au] to NiO.

The metal oxide nanofibers and/or metal-doped metal oxide nanofibers are disposed over a surface of an electrode. The electrode can be, for example, a gold, silver, platinum, copper, glassy carbon, or pyrolytic carbon electrode. In certain embodiments, the electrode is a gold electrode. In certain embodiments, the electrode is a silver electrode. In certain embodiments, the electrode is a platinum electrode. In certain embodiments, the electrode is a copper electrode. In certain embodiments, the electrode is a glassy carbon electrode. In certain embodiments, the electrode is a pyrolytic carbon electrode.

The non-enzymatic glucose sensor further comprises an alkaline solid electrolyte in contact with at least a portion of the metal oxide nanofibers and/or metal-doped metal oxide

nanofibers. The alkaline solid electrolyte provides an alkaline environment for glucose oxidation (similar to having an alkaline solution); and, when nanoporous, can block large particles like red cells and allows soluble materials in the blood, such as glucose, to flow through and be oxidized at the electrode surface, thus greatly improving the sensitivity and accuracy.

Thus, the alkaline solid electrolyte can be any solid electrolyte which can provide an alkaline pH at the location of the nanofibers (e.g., pH about 8 to about 14; in certain embodiments, a pH of about 10 to 13; in certain other embodiments, a pH of about 12 to about 13). Examples of suitable alkaline solid electrolytes include, but are not limited to, a sulfonated tetrafluoroethylene polymer, sodium hydroxide, and/or potassium hydroxide. Sulfonated tetrafluoroethylene polymers can include Nafion® 117 [CAS No 31175-20-9] a sulfonated tetrafluoroethylene based fluoropolymer-copolymer, {a copolymer of 2-[1-[difluoro-[(trifluoroethenyl)oxy]methyl]-1,2,2,2-tetrafluoroethoxy]-1,1,2,2,-tetrafluoroethane-1-sulfonic acid with tetrafluoroethylene}. In other embodiments, the alkaline solid electrolytes are sodium hydroxide or potassium hydroxide. The alkaline solid electrolyte may be nanoporous, as noted above, to act as a size-exclusion filter at the site of the metal oxide nanofibers and/or metal-doped metal oxide nanofibers.

Of these materials described above, glucose sensors made of metal-doped metal oxide nanofibers (e.g., NiO-Ag nanofibers) have shown higher sensitivity, lower detection limit, and wider linear range for glucose detection compared to sensors made of the individual components (e.g., NiO nanofibers or porous Ag). In particular, NiO-Ag sensors displayed a synergistic effect between NiO and Ag.

The non-enzymatic glucose sensors can be prepared according to a method comprising, depositing one or more metal oxide nanofibers and an alkaline solid electrolyte on an electrode surface, wherein the metal oxide nanofibers are optionally metal doped.

The nanofibers and electrolyte can be deposited by either (i) depositing the optionally metal-doped metal oxide nanofibers over a surface of the electrode and depositing the alkaline solid electrolyte over the optionally metal-doped metal oxide nanofibers; or (ii) co-depositing the optionally metal doped metal oxide nanofibers and an alkaline solid electrolyte on the electrode surface.

In an exemplary process, a suspension of nanofibers (e.g., Co_3O_4 nanofibers) can be cast onto the surface of an electrode (e.g., a glassy fiber electrodes (GCE)), and then the nanofibers can be entrapped by casting Nafion over the nanofibers to prepare a Co_3O_4 nanofiber-modified electrode. In another exemplary process, a suspension of nanofibers

(e.g., Co_3O_4 nanofibers) and an alkaline solid electrolyte can be co-cast onto the surface of an electrode (e.g., a glassy fiber electrodes (GCE)). "Depositing" and "casting" can each include drop casting, spray coating, screen printing, doctor-blading, and any other methods familiar to those skilled in the art for coating a surface with a solution.

The nanofibers described in any of the preceding aspects of the disclosure, and any embodiment thereof, can be formed by electrospinning a solution comprising at least one metal oxide precursor, one or more optional metal precursors, and a polymer to yield polymer composite fibers and calcining the polymer composite fibers under conditions suitable for removing the polymer from the nanofibers. The solvent can comprise water or an alcohol (e.g., methanol, ethanol, n-butanol, t-butanol, and the like). In certain embodiments, the solvent is a water and alcohol mixture (e.g., water and ethanol).

Electrospinning can utilize a spinneret (typically a hypodermic syringe needle) connected to a high-voltage (5 to 50 kV, e.g., 20 kV) direct current power supply, a syringe pump, and a grounded collector. A polymer solution, sol-gel, particulate suspension or melt is loaded into the syringe and this liquid is extruded from the needle tip at a constant rate suitable for the generation of fibers (e.g., 0.3 mL/h) by a syringe pump.

Calcination includes heating the polymer composite fibers at a temperature greater than 500 °C in an oxygen-containing atmosphere (e.g., air), for an amount of time suitable to remove the polymer from the fibers, to provide the desired nanofibers, as described above. In certain embodiments, the polymer composite fibers are heated to a temperature of at least about 500 °C for at least 3 hours (e.g., 3 – 10 hours; or 3- 5 hours).

Metal oxide precursors and metal precursors may include any metal salt familiar to those skilled in the art which is suitable for preparation of the desired optionally-doped metal oxide nanofibers. Suitable precursor salts include, Co(II) salts (e.g., $Co(NO_3)_2{\cdot}6H_2O$, $CoSO_4{\cdot}7H_2O$, $CoCl_2{\cdot}6H_2O$, and/or cobalt (II) acetate), Ni(II) salts (e.g., $Ni(NO_3)_2{\cdot}6H_2O$, $NiSO_4{\cdot}7H_2O$, $NiCl_2{\cdot}6H_2O$, and/or nickel (II) acetate), Ag(I) salts ($AgNO_3$, Ag_2SO_4, and/or silver acetate), Cd(II) salts ($Cd(NO_3)_2{\cdot}4H_2O$, $CdCl_2{\cdot}2.5H_2O$, $CdSO_4{\cdot}8/3H_2O$, and/or cadmium(II) acetate), Cu(II) salts (e.g., $Cu(NO_3)_2{\cdot}2.5H_2O$, $CuSO_4{\cdot}xH_2O$, $CuCl_2{\bullet}H_2O$, and/or copper(II) acetate), Au(III) salts (gold(III) chloride, gold(III) bromide, and/or $HAuCl_4{\cdot}3H_2O$), Pt(II) salts (e.g., platinum(II) iodide, platinum(II) bromide, and/or platinum(II) chloride), Pt(IV) salts (e.g., hydrogen hexahydroxyplatinate(IV) and/or platinum(IV) chloride), and/or Pd(II) salts (e.g., palladium(II) nitrate, palladium(II) sulfate, palladium(II) acetate, palladium(II) chloride, and/or palladium(II) bromide); Zn(II) salts (e.g., $ZnCl_2$, zinc(II) acetate, $Zn(NO_3)_2{\cdot}xH_2O$, $ZnBr_2$, ZnI_2, and/or $ZnSO_4{\cdot}7H_2O$), Sn(II) salts (e.g., $SnCl_2$ and/or

$SnBr_2$), Sn(IV) salts (e.g., $SnCl_4$, $SnBr_4$, and/or $SnBr_4$), Ce(III) salts (e.g., $CeBr_3$, $Ce_2(CO_3)_3 \cdot xH_2O$, $CeCl_3$, $Ce(NO_3)_3 \cdot 6H_2O$, and/or $Ce_2(SO_4)_3 \cdot xH_2O$), Ce(IV) salts (e.g., $Ce(OH)_4$ and/or $Ce(SO_4)_2 \cdot xH_2O$), Mn(II) salts (e.g., $MnCO_3$, $MnBr_2$, $Mn(NO_3)_2 \cdot xH_2O$, and/or $MnSO_4 \cdot xH_2O$), Ru(III) salts (e.g., $RuCl_3$, $Ru(NO)Cl_3 \cdot xH_2O$, and/or $RuI_3 \cdot H_2O$). Any of the preceding hydrated salts may also be used in their anhydrous forms.

For example, for preparing a metal-doped metal oxide nanofibers, the metal oxide precursor can be one or more Co(II) salt, Ni(II) salt, Cd(II), and/or Cu(II) salt; and the metal precursor can be one or more Ag(I) salt, Au(III) salt, Pt(II) salt, Pt(IV) salt, and/or Pd(II) salt.

In another example, for preparing metal-doped NiO nanofibers, the metal oxide precursor can be one or more Ni(II) salt; and the metal precursor can be one or more Ag(I) salt, Au(III) salt, Pt(II) salt, Pt(IV) salt, and/or Pd(II) salt (e.g,. Ag(I) salt for Ag-NiO nanofibers; Au(III) salt for Au-NiO nanofibers, Pt(II) or Pt(IV) salt for Pt-NiO nanofibers; and Pd(II) salt for Pd-NiO nanofibers).

In another example, for preparing metal-doped Co_3O_4 nanofibers, the metal oxide precursor can be one or more Co(II) salt; and the metal precursor can be one or more Ag(I) salt, Au(III) salt, Pt(II) salt, Pt(IV) salt, and/or Pd(II) salt (e.g,. Ag(I) salt for Ag-Co_3O_4 nanofibers; Au(III) salt for Au-Co_3O_4 nanofibers, Pt(II) or Pt(IV) salt for Pt-Co_3O_4 nanofibers; and Pd(II) salt for Pd-Co_3O_4 nanofibers).

Suitable polymers include, but are not limited to, poly(vinyl pyrrolidone) (PVP), poly(acrylic acid) (PAA), poly(caprolactone) (PCL), poly(vinyl alcohol) (PVA), poly (vinyl acetate) (PVAc), and poly(ethylene oxide) (PEO). In certain embodiments, the polymer is PVP. The polymer (e.g., PVP) can have any molecular weight which is soluble in the desired solution and which can form the desired nanofibers, such as, greater than about 1,000,000 Da molecular weight (e.g., about 1,300,000 Da molecular weight). "Molecular weight" as used herein refers to weight-averaged molecular weight as is familiar to those skilled in the art.

The polymer composite fibers can have average diameters between about 10 nm and about 1000 nm. In certain embodiments, the polymer composite fibers can have an average diameter between about 100 nm and about 500 nm. In other embodiments, the polymer composite fibers can have an average diameter between about 100 nm and about 350 nm.

After calcination, nanofibers are formed having average diameters between about 50 nm and about 200 nm. In another embodiment, the nanofibers have average diameters between about 50 nm and about 150 nm. In another embodiment, the nanofibers have

average diameters between about 50 nm and about 100 nm. In another embodiment, the nanofibers have average diameters between about 50 nm and about 75 nm.

The preceding non-enzymatic glucose sensor according to any of the preceding embodiments can be incorporated into a glucose detection apparatus (e.g. glucose meter, potentiostat). The apparatus may comprise a temperature sensor positioned to detect the temperature at or near a surface of the non-enzymatic glucose sensor. The glucose detection apparatus may also comprise programmed software to calibrate for a temperature effect on performance of the non-enzymatic glucose sensor. As the temperature effect on sensor performance can be calibrated using a temperature sensor and programmed software, the present sensors can be used in many places where there is no temperature control.

The sensor of the present invention can be fabricated as a test strip similar to glucose oxidase-based test strips, thus fabricating facilities used for the glucose oxidase based test strips can be used for the fabrication of the non-enzymatic test strips of the present invention. Thus, in another aspect, glucose test strips are provided comprising a non-enzymatic glucose sensor of any of the preceding aspects and embodiments of the disclosure. The test strips can comprise, a working electrode having a coating, wherein the coating comprises a metal oxide nanomaterial and an alkaline solid electrolyte, and wherein the metal oxide nanomaterial is optionally metal doped.

The test strip may further comprise a counter electrode and a reference electrode, each positioned in electrochemical communication with the working electrode. That is, the test strip can comprise a non-enzymatic glucose sensor as described above, a counter electrode, and a reference electrode.

The test strips also comprise a support material which is capable of conveying an aqueous test sample (e.g., blood or plasma) from a first point on the material (a sample application point) to the non-enzymatic glucose sensor at a second point on the material. Such support materials include paper, nylon, plastic, or a filter, and can be a suitable size for its intended purpose. Other examples of such support materials include wicking membranes, such as cellulose membranes, nitrocellulose membranes, or microfluidic devices which convey the aqueous test sample to aqueous test sample via one or more microfluidic channels leading from the first point on the material (sample application point).

It is a further feature of the present invention that a conventional glucose meter can be adapted for use with the metal oxide-based non-enzymatic test strip described herein.

In one embodiment metal oxide nanofibers and alkaline solid electrolytes are applied to strips by a screen printing process. In one embodiment metal oxide nanofibers and alkaline solid electrolytes are applied to strips by a spray coating process.

EXAMPLES

Example 1 *Co_3O_4 nanofibers*

Cobalt nitrate hexahydrate ($Co(NO_3)_2 \cdot 6H_2O$) and sodium hydroxide (NaOH, pellets) were purchased from Fisher Scientific. Human serum (from male AB clotted whole blood), Nafion® 117 solution (purum, ~5% in a mixture of lower aliphatic alcohols and water) and Poly(vinyl pyrrolidone) (PVP, MW = 1,300,000) were obtained from Sigma-Aldrich. Ascorbic acid, uric acid, ethanol (for HPLC, denatured) and D-(+)-glucose were supplied by Acros Organics. 0.1 M pH 7.0 phosphate buffer solution was prepared using Na_2HPO_4 and NaH_2PO_4. Glucose solutions with different concentrations were diluted from stock solution (1 M). All aqueous solutions were prepared with deionized water (18.2 MΩ-cm) generated by a Barnstead water system.

0.4 g $Co(NO_3)_2 \cdot 6H_2O$ was dissolved in 1.6 g water and 0.4 g PVP was dissolved in 2.4 g ethanol, respectively. The two solutions were then mixed and kept under magnetic stirring for at least 1 h. The as-prepared homogenous solution was electrospun using a 19-gauge needle with a flow rate of 0.3 mL/h at an applied voltage of 20 kV over a collection distance of 15 cm. The fibers were collected on aluminum foil and then calcined under an air atmosphere at 500 °C for 3 hours in order to remove the matrix polymer and generate Co_3O_4 nanofibers.

Example 2 *Co_3O_4 nanofibers modified electrode*

Before surface modification, glassy carbon electrode (GCE, dia. 3 mm) was polished with 1 μm and 0.05 μm alumina slurries sequentially, and then rinsed with DI water. Finally, the electrode was sonicated in ethanol and deionized water, dried at room temperature, and ready for modification. To prepare 5 mg/mL Co_3O_4 nanofibers suspension, 5 mg Co_3O_4 nanofibers was first suspended in 1 mL ethanol and sonicated for 1 hour, and then a 5 μL suspension was dropped onto the surface of GCE. After drying in air, an aliquot of 5 μL Nafion solution (1 wt% in ethanol) was casted on the layer of Co_3O_4 nanofibers in order to entrap Co_3O_4. The as-prepared electrode (denote as Co_3O_4 NFs-Nafion/GCE) was immersed in water for 1 h to wet the Nafion layer thoroughly before use. The Nafion coated GCE (Nafion/GCE) was also prepared as a control electrode.

Example 3 *Characterization of Co_3O_4 nanofibers*

A JEOL 6335F field-emission scanning electron microscope was used to examine the morphology and the size of the as-electrospun precursor nanofibers and Co_3O_4 nanofibers. More detailed morphology and selected area electron diffraction (SAED) patterns were obtained with a Tecnai T12 transmission electron microscope operated at 120 kV. XRD patterns were obtained with an Oxford diffraction XcaliburTM PX Ultra with ONYX detector to study the crystal structure of Co_3O_4 nanofibers. FTIR spectra were obtained on a Nicolet Magna-IR 560 spectrophotometer (Bruker, Germany). Raman spectra were recorded at ambient temperature on a Renishaw Ramanscope Micro-Raman with 514 nm wavelength laser. Cyclic voltammetry (CV) measurements were performed on a Model CHI 601C Electrochemical Workstation (CH Instruments, USA). All experiments were conducted using a three-electrode electrochemical cell (working volume of 5 mL) with a working electrode, an Ag/AgCl reference electrode, and a platinum disc counter electrode. For amperometric detection, all measurements were performed by applying an appropriate potential to the working electrode and allowing the transient background current to decay to a steady-state value, before the addition of the analyte. A stirred solution was employed to provide convective transport.

The SEM images of PVP/$Co(NO_3)_2$ composite nanofibers and the Co_3O_4 nanofibers obtained after calcination at 500 °C are shown in **Fig. 1A** and **1B**, respectively. One can see that the fiber morphology was maintained after the degradation of PVP and decomposition of $Co(NO_3)_2$, accompanied by a decrease of an average diameter from 302 ± 25 nm to 105 ± 10 nm (calculated from 50 randomly selected nanofibers under SEM images), which was attributed to the loss in total mass upon calcination. Unlike the smooth surface of precursor nanofibers (**Fig. 1A**), the nanofibers obtained after calcination were composed of numerous nanoparticles with relatively uniform distribution and their surfaces are not smooth any more (**Fig. 1B** and **1D**), which provide even larger accessible surface area for the subsequent electrochemical catalytic reaction of glucose. The SAED pattern (inset in **Fig. 1D**) indicates the crystalline structure of the as-prepared Co_3O_4 nanofibers. After sonication in ethanol for 1 hour, long Co_3O_4 nanofibers were exfoliated to short nanofibers with an average length of ca. 1 μm and a three dimensional (3D) porous network was formed after drop-casting the sonicated sample on solid substrate (**Fig. 1C**).

Fig. 2A shows the FTIR spectra of the electrospun precursor nanofibers and the obtained Co_3O_4 nanofibers, respectively. Two sharp peaks at 663 and 571 cm^{-1} were observed in the spectrum of Co_3O_4 nanofibers while the characteristic peaks of PVP (e.g. 1654 cm^{-1} for C=O)

and $Co(NO_3)_2$ (e.g. 1381 cm^{-1} for NO_3^-) did not existed in the spectrum. The two sharp peaks can be assigned to Co-O bonds existing in Co (II, III) oxide. The disappearance of the characteristic peaks of PVP and $Co(NO_3)_2$ is an indication of the complete degradation of PVP and the conversion of $Co(NO_3)_2$ to Co_3O_4. Raman spectra were employed to further examine the difference between the precursor nanofibers and the final product. As shown in **Fig. 2B** (curve b), four peaks located at 483, 523, 621, and 694 cm^{-1}, corresponds to E_g, F^1_{2g}, F^2_{2g}, and A^1_g modes of the crystalline Co_3O_4, respectively. As a comparison, the Raman spectrum of the precursor nanofibers does not show any obvious peak (curve a).

The crystal structure and the phase purity of the as-prepared Co_3O_4 nanofibers were further characterized by XRD. As shown in **Fig. 3A**, the XRD spectrum of Co_3O_4 nanofibers matches the standard spectrum of cubic crystalline Co_3O_4 (JCPDS 42-1467). The formation of cubic crystalline Co_3O_4 is revealed by the diffraction peaks at 2θ values of 19.00, 31.27, 36.85, 38.54, 44.81, 56.66, 59.36, 65.24, 74.12° corresponding to (111), (220), (331), (222), (440), (422), (511), (440), and (620) crystal planes, respectively. No other impurities could be detected in the XRD pattern of Co_3O_4, indicating that pure Co_3O_4 is obtained. XPS measurement was carried out to further confirm the presence of Co_3O_4. As demonstrated in **Fig. 3B**, the two peaks located at binding energies of 780.24 eV and 795.52 eV with a separation of 15.28 eV correspond to Co $2p_{3/2}$ and Co $2p_{1/2}$ orbit of Co_3O_4, respectively.

Example 4 *Electrochemical behavior of the Co_3O_4 NFs-Nafion/GCE*

The CVs of the Co_3O_4 NFs-Nafion/GCE were investigated in both alkaline solution (0.1 M NaOH) and neutral solution (0.1 M pH 7.0 phosphate buffer) in the range from 0 to 0.7 V vs. Ag/AgCl (**Fig. 4A**). No obvious oxidation or reduction peak was observed in the neutral electrolyte while two pairs of well-defined redox peaks were obtained in alkaline solution. This phenomenon indicates the involvement of OH^- in the electrochemical redox reaction of Co_3O_4. As labeled in **Fig. 4A**, the pair of redox peaks I/II can be assigned to the reversible transition between Co_3O_4 and CoOOH, while another pair of redox peaks III/IV can be attributed to further conversion between CoOOH and CoO_2. These two reversible reactions can be schematically expressed as equation (1) $Co_3O_4 + OH^- + H_2O \leftrightarrow 3CoOOH + e^-$ and equation (2) $CoOOH + OH^- \leftrightarrow CoO_2 + H_2O + e^-$.

The dependence of peak currents on scan rates was presented in **Fig. 4B**. The redox peak currents increased linearly with the scan rate in the range from 25 to 200 mV/s (**Fig. 4C**), indicating a surface-controlled electrochemical process.

Example 5 *Electrooxidation of glucose at the Co_3O_4 NFs-Nafion/GCE*

Following a facile two-step synthesis route (electrospinning and subsequent calcination), Co_3O_4 nanofibers with average diameter of ca. 105 nm were fabricated. Raman and FTIR spectra were performed to confirm the complete decomposition of polymer matrix and decomposition cobalt salt. XRD and XPS were employed to study the crystal structure and composition of the oxide. The Co_3O_4 nanofibers suspension was casted onto the surface of GCE and then entrapped with Nafion to prepare Co_3O_4 nanofibers modified GCE. The Co_3O_4 NFs-Nafion/GCE showed two pairs of well-defined redox peaks in alkaline electrolyte but no obvious redox peaks in neutral solution. The Co_3O_4 nanofibers based non-enzymatic glucose sensor showed excellent performance towards the electrooxidation of glucose in alkaline solution. Its application to human blood serum was also demonstrated. The low detection limits, high reproducibility, and good selectivity of the as-prepared glucose sensor make Co_3O_4 nanofibers a good candidate for the construction of non-enzymatic sensor for glucose detection. In addition, Langmuir isothermal theory was applied to fit the calibration curve. The mechanisms for glucose detection and good selectivity were also discussed.

The electrooxidation of glucose at the Co_3O_4 NFs-Nafion/GCE was first examined in 0.1 M NaOH solution. **Fig. 5A** presents the CVs in the absence and presence of 2.8 mM glucose, recorded at the Nafion-GCE (curves a and b) and the Co_3O_4 NFs-Nafion/GCE (curves c and d), respectively. The Co_3O_4 NFs-Nafion/GCE exhibited significant oxidation of glucose starting at ca. +0.25 V and covering the potential region where CoOOH and CoO_2 are formed. By contrast, no obvious response was found at the Nafion/GCE. The result indicated that the catalytic property of the as-prepared Co_3O_4 nanofibers towards glucose oxidation in alkaline solution was related to CoOOH and CoO_2. In addition, as shown in **Fig. 5A**, the current increase with the addition of glucose at peak III ($CoOOH \rightarrow CoO_2$) was much stronger than that at peak I ($Co_3O_4 \rightarrow CoOOH$), which may suggest that the electrooxidation of glucose is mainly mediated by $CoOOH/CoO_2$ rather than $Co_3O_4/CoOOH$ in an alkaline solution. Therefore, the peak III potential was applied for subsequent amperometric detection. It is widely accepted that glucose can be oxidized to produce gluconolactone through 2-electron electrochemical reaction. Therefore, the mechanism of glucose electrochemical oxidation reaction catalyzed by Co_3O_4 nanofibers at peak III (+0.59 V) can be presumably proposed according to the following equation (3) $2CoO_2 + C_6H_{12}O_6$ (glucose) $\rightarrow$ $2CoOOH + C_6H_{10}O_6$ (gluconolactone). With the consumption of CoO_2 and the production of CoOOH, the extent of Reaction (2) ($CoOOH + OH^- \leftrightarrow CoO_2 + H_2O + e^-$) would greatly favor the forward reaction

($CoOOH \rightarrow CoO_2$), thus resulting in an enhanced oxidation peak III upon the addition of glucose (**Fig. 5A**).

In addition, no response to glucose was observed at the as-prepared Co_3O_4 NFs-Nafion/GCE when the same experiment was carried out in neutral buffer solution (data not shown), indicating the critical role of OH^- in the glucose oxidation. The experimental observation is in good agreement with Equations (1)-(3).

As the oxidation (anodic) peak current at ca. +0.59 V increases significantly with the increase of glucose concentration, an applied potential of +0.59 V (peak potential of peak III) was applied to conduct non-enzymatic amperometric detection of glucose in 0.1 M NaOH solution. As shown in **Fig. 5B**, the non-enzymatic glucose sensor exhibited a rapid (reaching 95% of steady-state current in less than 7 s) and sensitive response to the addition of glucose. The indicated concentration in **Fig. 5B** has considered the dilution effect. The slight baseline drift was observed after multiple injections of glucose, which may be attributed to small variation of local pH, the faster glucose consumption than its diffusion, or the adsorption of intermediates on the active sites. The corresponding calibration curve (**Fig. 5C**) is linear up to 2.04 mM with a sensitivity of 36.25 $\mu A\ mM^{-1}\ cm^{-2}$ and a detection limit of 0.97 μM (S/N = 3), but saturated at a higher glucose concentration. The obtained sensitivity is better than those of 17.8 $\mu A\ mM^{-1}\ cm^{-2}$ at Pt-Pb alloy nanoparticles-MWCNTs/GCE (Cui, H.F. et al., 2007. Anal. Chim. Acta 594, 175-183), 11.8 $\mu A\ mM^{-1}\ cm^{-2}$ at porous Au electrode (Li, Y. et al., 2007. Electrochem. Commun. 9, 981-988), 4.36 $\mu A\ mM^{-1}\ cm^{-2}$ at MWCNTs electrode (Ye, J.S. et al., 2004. Electrochem. Commun. 6, 66-70), and 9.6 $\mu A\ mM^{-1}\ cm^{-2}$ at mesoporous Pt electrode (Park, S. et al., 2003. Anal. Chem. 75, 3046-3049). In addition, the detection limit is among the lowest reported values for non-enzymatic glucose sensors (Jiang, L.C., Zhang, W.D., 2010. Biosens. Bioelectron. 25, 1402-1407; Lu, L.M. et al., 2009. Biosens. Bioelectron. 25, 218-223; Ozcan, L. et al., 2008. Biosens. Bioelectron. 24, 512-517; Reitz, E. et al., 2008. Electroanalysis 20, 2482-2486; Safavi, A. et al., 2009. Biosens. Bioelectron. 24, 1655-1660; Wang, W. et al., 2009. Biosens. Bioelectron. 25, 708-714). The high sensitivity and low detection limit can be attributed to the excellent catalytic property of the as-prepared Co_3O_4 nanofibers and the highly porous 3D network of Co_3O_4 nanofibers, which provides high specific surface area and numerous active sites, and also allows the access of analytes to the active catalytic sites with minimal diffusion resistance (Jia, W.Z. et al., 2008. Electroanalysis. 20, 2153-2157; Jia, W.Z. et al., 2009. J. Electroanal. Chem. 625, 27-32).

The electrochemical oxidation of glucose on Co_3O_4 nanofibers is a surface catalytic reaction. Therefore, Langmuir isothermal theory was used to fit the calibration curve (**Fig. 5C**). According to the Langmuir isotherm theory, the concentration of glucose adsorbed on the catalyst surface ($C_{\text{glucose·S}}$) can be expressed as:

$$C_{glucose\cdot S} = \frac{K_A C_{\text{glucose}} C_t}{1 + K_A C_{\text{glucose}}}$$

where C_{glucose} is the concentration of glucose in the bulk electrolyte, C_t is the total molar concentration of active sites on Co_3O_4 nanofibers which is constant, and K_A is the adsorption equilibrium constant. Therefore, at a given applied potential, the current response I from glucose electrochemical oxidation for a good approximation is proportional to $C_{\text{glucose·S}}$ with a rate constant of K_B, thus I can be expressed as follows by defining a new constant $K = K_A K_B C_t$:

$$I = K_B C_{glucose\cdot S} = \frac{K_A K_B C_t C_{glucose}}{1 + K_A C_{glucose}} = \frac{K C_{glucose}}{1 + K_A C_{glucose}}$$

As shown in **Fig. 5C**, the calibration data fit into this equation very well (R = 0.994) with K= 2.557 and K_A= 0.08323, thus I can be expressed as follows.

$$I = \frac{2.557 C_{glucose}}{1 + 0.08323 C_{glucose}}$$

When glucose concentration is low (i.e. $0.08323 C_{glucose} << 1$), the equation above can be approximated as I = 2.557 $C_{glucose}$. Thus the sensitivity is calculated to be 36.17 μA mM^{-1} cm^{-2}, which is in good agreement with the previous result (36.25 μA mM^{-1} cm^{-2}) if only linear range is considered. In addition, the investigation of the dissociative adsorption model is also conducted (data not shown) and the result suggests that glucose does not dissociate upon adsorption onto the active sites on Co_3O_4 nanofibers and is mainly consumed by the electrooxidation process.

The proposed sensor was further applied to the detection of glucose in human blood serum sample. **Fig. 5D** demonstrated the amperometric response to successive three repeated additions of analytes in the sequence of 5 μL blood serum sample, 5 μL 10 mM glucose in buffer, 10 μL blood serum sample, and 10 μL 10 mM glucose in buffer. The concentration of glucose in human blood serum sample was calibrated by standard glucose solution and the result was presented in the inset table in **Fig. 5D**. The same serum sample was also measured by commercial glucose meter (OneTouch UltraMini, LifeScan, Inc, CA). The good

agreement between the results obtained by our proposed sensor and those read from the commercial glucose detector indicates the practical application of the as-prepared non-enzymatic glucose sensor.

The selectivity of the Co_3O_4 NFs-Nafion/GCE was also investigated against normally co-existed interfering species with glucose such as ascorbic acid (AA) and uric acid (UA). The blood glucose level of a normal human body is between 4 and 7 mM, while the concentration of endogenous AA and UA is respectively about 0.125 mM and 0.33 mM in blood samples. As demonstrated in **Fig. 6C**, 0.125 mM AA dissolved in 4 mM glucose solution can only result in 14% increase of amperometric response compared to the response for 4 mM glucose, while 0.33 mM UA leads to 17% increase, which is not significant. However, the responses obtained at the Co_3O_4 NFs-Nafion/GCE to 0.125 mM AA and to 0.33 mM UA alone are 23.16% and 33.70% of that of 4 mM glucose, respectively, which is much higher than the observed percentage increase caused by UA in glucose/UA or AA in glucose/AA. Our study showed that the charge-exclusion property of Nafion coating layer cannot eliminate the interference of UA and AA at +0.59 V vs. Ag/AgCl because the response of the control electrode (Nafion/GCE) to 0.125 mM AA and 0.33 mM UA are more than 6 folds higher than that of 4 mM glucose (**Fig. 6B**). Therefore, such good selectivity against UA and AA at +0.59 V vs. Ag/AgCl at the Co_3O_4 NFs-Nafion/GCE can be hypothesized as the repelling effect described in **Fig. 6A**. Co_3O_4 has an isoelectric point (IEP) of ~ 8. In 0.1 M NaOH solution (pH = 13), the Co_3O_4 nanofibers surfaces would be negatively charged. UA and AA would also be negatively charged in 0.1 M NaOH solution due to the loss of proton. Consequently, the negatively charged Co_3O_4 nanofibers surface could strongly repel the negatively charged UA and AA molecules, thus greatly reducing the electrooxidation of UA and AA on the surface of Co_3O_4 nanofibers at an applied potential of +0.59 V and resulting in good selectivity.

Since chloride ions can poison most of the non-enzymatic glucose sensors based on precious metals and alloys, the amperometric response of the Co_3O_4 NFs-Nafion/GCE to 4 mM glucose was examined in the presence and absence of 0.1 M NaCl in 0.1 M NaOH solution. It was observed that the response at the Co_3O_4 NFs-Nafions/GCE remains unchanged, implying that the Co_3O_4 nanofibers modified electrode can work well for the sample with high concentration of chloride ions (e.g. blood sample).

The reproducibility of the developed biosensor for glucose was also investigated. The relative standard deviation (R.S.D) of 3.99% (n = 5) for 80 μM glucose demonstrated good intra-electrode reproducibility. Additionally, the good electrode-to-electrode reproducibility

was characterized by the low R.S.D of 9.73% in the response to 4 mM glucose on five Co_3O_4 NFs-Nafions/GCE sensors. These results should make the Co_3O_4 nanofibers an ideal material for the construction of non-enzymatic glucose biosensor.

Example 6 *Preparation of NiO-Ag nanofibers, NiO nanofibers, and porous Ag*

Nickel nitrate hexahydrate ($Ni(NO_3)_2 \cdot 6H_2O$), silver nitrate ($AgNO_3$) and D-(+)-glucose were purchased from Acros Organics. Sodium hydroxide (NaOH) was supplied by Fisher Scientific. Human serum (from male AB clotted whole blood) and poly(vinyl pyrrolidone) (PVP, MW = 1,300,000) were obtained from Sigma-Aldrich. 0.1 M pH 7.0 phosphate buffer solution was prepared using Na_2HPO_4 and NaH_2PO_4. All aqueous solutions were prepared with deionized water (18.2 MΩ-cm) generated by a Barnstead water system.

0.4 g $Ni(NO_3)_2 \cdot 6H_2O$ and 0.1 g $AgNO_3$ were dissolved in 1.6 g water and then mixed with a 2.8 g solution consisting of 0.4 g PVP and 2.4 g ethanol. The $Ni(NO_3)_2$-$AgNO_3$-PVP composite nanofibers were prepared using a 23-gauge needle with a flow rate of 0.3 mL/h at an applied voltage of 20 kV over a gap distance of 15 cm and were collected on aluminum foil. The precursor was then calcined under air atmosphere at 500 °C for 3 h in order to remove the matrix polymer and generate NiO-Ag nanofibers.

NiO nanofibers and porous Ag were also synthesized following the similar procedure, the only difference was using 0.4 g $Ni(NO_3)_2 \cdot 6H_2O$ or 0.1 g $AgNO_3$ as the only metal precursor, respectively.

Example 7 *Preparation of NiO-Ag nanofibers, NiO nanofibers, and porous Ag modified electrodes*

Before surface modification, glassy carbon electrode (GCE, dia. 3 mm) was polished with 1 μm and 0.05 μm alumina slurries sequentially, and then rinsed with deionized (DI) water. Finally, the electrode was sonicated in ethanol and deionized water, dried at room temperature, and ready for modification. To prepare 5 mg/mL NiO-Ag nanofibers suspension, 5 mg NiO-Ag nanofibers was first suspended in 1 mL ethanol and sonicated for 1 hour, and then a 5 μL suspension was dropped onto the surface of GCE. After drying in air, an aliquot of 5 μL Nafion solution (1 wt% in ethanol) was casted on the layer of NiO-Ag nanofibers in order to entrap NiO-Ag nanofibers. The as-prepared electrode (denote as NiO-Ag NFs/GCE) was immersed in water for 1 hour to wet the Nafion layer thoroughly before use. Similar procedure was also applied to prepare NiO nanofibers or porous Ag modified GCEs (NiO NFs/GCE and porous Ag/GCE).

Example 8 *Characterization of NiO-Ag nanofibers, NiO nanofibers, and porous Ag*

A JEOL 6335F field-emission scanning electron microscope was used to examine the morphology and the size of the as-prepared samples. More detailed morphology and selected area electron diffraction (SAED) patterns were obtained with a Tecnai T12 transmission electron microscope operated at 120 kV. XRD patterns were obtained with an Oxford diffraction XcaliburTM PX Ultra with ONYX detector to study the crystal structure of the NiO-Ag nanofibers. FTIR spectra were obtained on a Nicolet Magna-IR 560 spectrophotometer (Bruker, Germany). The surface property of the sample was analyzed by X-ray photoelectron spectroscopy (XPS) with a PHI multiprobe using Mg as the exciting source. Cyclic voltammetry (CV) measurements were performed on a Model CHI 601C Electrochemical Workstation (CH Instruments, USA). All experiments were conducted using a three-electrode electrochemical cell with a working electrode, an Ag/AgCl reference electrode, and a platinum disc counter electrode. For amperometric detection, all measurements were performed by applying an appropriate potential to the working electrode and allowing the transient background current to decay to a steady-state value, before the addition of the analyte. A stirred solution was employed to provide convective transport.

SEM was first performed to investigate the morphology of the precursor nanofibers and the corresponding calcined products. **Fig. 7a, c, e** presents the images of three different precursors, $AgNO_3$-PVP, $Ni(NO_3)_2$-PVP and $Ni(NO_3)_2$-$AgNO_3$-PVP nanofibers, respectively. The average diameter of each precursor nanofiber was calculated based on 50 randomly selected nanofibers and listed in **Table 1**. Compared to the nanofibers prepared by single metal salt with PVP, the nanofibers electrospun from PVP containing two mixed metal salts had a smaller average diameter (ca. 20 nm smaller). This might be resulted from the increase of solution conductivity. After calcined under air atmosphere for 3 hours, the polymer matrix was totally degraded. $AgNO_3$ and $Ni(NO_3)_2$ were decomposed following the reactions below:

$$2AgNO_3 \xrightarrow{\Delta} 2Ag + 2NO_2 \uparrow + O_2 \uparrow \quad (1) \qquad 2Ni(NO_3)_2 \xrightarrow{\Delta} 2NiO + 4NO_2 \uparrow + O_2 \uparrow \quad (2)$$

Table 1. Average diameters of nanofibers (NFs) before and after calcination

	$AgNO_3$-PVP NFs (nm)	Porous Ag	$Ni(NO_3)_2$-PVP NFs (nm)	NiO NFs (nm)	$Ni(NO_3)_2$-$AgNO_3$-PVP NFs (nm)	NiO-Ag NFs (nm)
Average Diameter (nm)	254.0 ± 29.7	—	249.4 ± 42.5	72.6 ± 22.6	230.4 ± 27.5	82.1± 13.8

Ag cannot maintain the nanofiber structure after calcination of $AgNO_3$-PVP nanofibers and some Ag merged together to form a porous network (**Fig. 7b**). In contrast, NiO still kept the nanofiber structure with a decrease in the average diameter from 249.4 ± 42.5 nm to 72.6 ± 22.6 nm, which was caused by the weight loss due to the decomposition. The surfaces of NiO nanofibers were no longer as smooth as the $Ni(NO_3)_2$-PVP nanofibers (**Fig. 7d**). As for NiO-Ag composite, the nanofiber structure was also maintained (**Fig. 7f**), but its average diameter was slightly larger than that of NiO nanofibers. This can be explained by the decrease of the percentage of PVP in the precursory electrospun nanofibers due to the introduction of $AgNO_3$.

TEM was also employed to characterize the nanofibers before and after calcination. As shown in **Fig. 8a**, numerous black dots, with an average diameter of 5.38±1.84 nm (calculated from 50 randomly selected nanoparticles), are well distributed in a single $Ni(NO_3)_2$-$AgNO_3$-PVP nanofiber. These black dots are Ag nanoparticles, which may come from the reduction of partial $AgNO_3$ dissolved in PVP-ethanol. The *in-situ* formation of Ag nanoparticles can be demonstrated by UV-Vis absorption spectra. An increase in the peak density located at ca. 436 nm (the surface Plasmon band resonance of Ag nanoparticles with sizes between 2-50 nm) indicates the gradually formation of Ag nanoparticles in precursor solution. Similar results were obtained with $AgNO_3$-PVP in ethanol solution (data not shown). These results indicate that $Ni(NO_3)_2$ co-presented with $AgNO_3$ in PVP-ethanol solution would not prohibit the formation of Ag nanoparticles.

The comparison between TEM images of a NiO nanofiber and a NiO-Ag hybrid nanofiber was presented in **Fig. 8b and 8c**. One can see that both nanofibers show uneven surfaces, however, NiO nanofiber was composed of larger nanoparticles, while the NiO-Ag hybrid nanofiber consists of numerous smaller nanoparticles. The elemental heterogeneity of NiO-Ag nanofiber was further examined by EDX mapping. The three insets in **Fig. 8c**

represent EDX mapping of Ag, Ni and O elements, respectively, in the selected area as indicated by the red dash frame. The recorded images of Ni and O mapping indicate a homogeneous distribution of NiO, while Ag shows an irregular distribution. Selected area electron diffraction (SAED) pattern shows the polycrystalline structure of the hybrid nanofibers.

The composition changes between the precursor nanofibers and the calcined products were revealed by EDX analysis (**Fig. 8e**). The increase in the ratio of Ni and Ag elements indicates the degradation of polymer matrix and decomposition of metal salts. The carbon peak presented in **Fig. 8e** and Cu peak in **Fig. 8e** and its inset can be attributed to the copper-carbon grid used for EDX.

FTIR was further performed to confirm the complete removal of polymer matrix and conversions of metal salts. As demonstrated in **Fig. 9a**, no characteristic peak was observed in the spectrum of porous Ag, while a sharp peak located at 435 cm^{-1} in both spectra of NiO and NiO-Ag hybrid nanofibers can be assigned to Ni-O bond. The characteristic peak of NO_3^- (1395 cm^{-1}) in $Ni(NO_3)_2$-$AgNO_3$-PVP and the peak of C=O (1650 cm^{-1}) in PVP disappeared after calcination, indicating the degradation of PVP and decomposition of nitrate salts. The presence of peaks at 3440 cm^{-1} and 1640 cm^{-1} may be due to the absorption of moisture during mixing and pelleting the samples with KBr, while the peak shown at 2360 cm^{-1} can be assigned to CO_2 from surrounding atmosphere.

The composition and crystal structure were further characterized by XRD (**Fig. 9b**). The XRD spectrum of NiO-Ag nanofibers matches the combination of the standard spectrum of JCPDS 04-0835 (NiO) and JCPDS 04-0783 (Ag). The formation of face-centered cubic crystalline NiO is revealed by the diffraction peaks at 2θ values of 37.28, 43.30, 62.92, 75.44, 79.39, 95.08° corresponding to (111), (200), (220), (311), (222), and (400) crystal planes, respectively; while the diffraction peaks at 2θ values of 38.12, 44.28, 64.43, 77.47, 81.54 and 97.89°, which correspond to (111), (200), (220), (311), (222), and (400) crystal planes respectively, indicates the formation of cubic crystalline Ag. XPS measurement was carried out to further confirm the valence state of Ni and Ag element in NiO-Ag hybrid nanofibers. As demonstrated in **Fig. 9c**, two main peaks presented at binding energies of 853.53 eV and 871.58 eV with a separation of 18.1 eV can be assigned to Ni $2p_{3/2}$ and Ni $2p_{1/2}$ orbit of NiO, respectively. In addition, three satellite (sat) peaks, due to final-state effects, are shown at 877.92, 860.12, and 855.68 eV, respectively. It is well accepted that Ni 2p photoelectron spectrum of NiO exhibits a very strong satellite structure. On the other hand, the two peaks

located at binding energies of 367.58 eV and 373.58 eV with a separation of 6.00 eV correspond to Ag $3d_{5/2}$ and Ag $3d_{3/2}$ orbit of Ag, respectively (**Fig. 9d**).

Example 9 *Electrochemical behavior of NiO-Ag NFs, NiO NFs, and porous Ag modified GCEs*

The electrocatalytic activities of the NiO-Ag NFs, NiO NFs, and porous Ag modified electrodes were compared. **Fig. 10a, b, c** presents the CVs of the three different electrodes in the absence and presence of 8 mM glucose in 0.1 M NaOH solution recorded at a scan rate of 100 mV/s, respectively. A pair of well-defined quasi-reversible redox peaks was observed at the NiO NFs/GCE, with the anodic peak potential at 0.516 V and the cathodic peak at 0.442 V (**Fig. 10a**, trace a). These two peaks are assigned to Ni^{2+}/Ni^{3+} redox couple. Upon the addition of 8 mM glucose, the anodic peak current increased (**Fig. 10a**, trace b), which can be attributed to the catalytic effect of the redox couple for oxidation of glucose to gluconolactone according to the following reactions:

$$NiO+OH^- + e^- \rightarrow NiO(OH) \quad (3)$$

$$2NiO(OH)+glucose \rightarrow 2NiO+gluconolactone+H_2O \quad (4)$$

When neutral buffer was used, these two peaks were not observed and no response towards glucose addition was obtained (data not shown), which indicates the critical role of OH^- in the reaction.

As for porous Ag/GCE, the oxidation peak (I) at ca. 0.325 V is attributed to the oxidation of Ag^0 to Ag^{1+} while the peak (II) at ca. 0.785 V is assigned to the oxidation of Ag^{1+} to Ag^{2+} (**Fig. 10b**). In the cathodic scan, the reductions of Ag^{2+} to Ag^{1+} and Ag^{1+} to Ag^0 appear at ca. 0.418 V and 0 V, respectively. In the presence of 8 mM glucose, the oxidation peak (I) positively shifted to 0.362 V and the peak (II) shifted to 0.825 V.

Compared to the NiO NFs and porous Ag modified electrodes, the NiO-Ag NFs/GCE exhibits a greatly enhanced background current (**Fig. 10c**). Well-defined oxidation and reduction peaks for Ag^0/Ag^{1+} and Ag^{1+}/Ag^{2+} redox couples are also presented, while the peaks for Ni^{2+}/Ni^{3+} redox couple can be hardly identified. A shoulder peak at ca. 0.6 V may be assigned to the oxidation of Ni^{2+} to Ni^{3+}. However, the reduction peak (III) becomes more obvious compared to that of the porous Ag/GCE (**Fig. 10b**), which may be due to the overlap of the reduction of Ni^{3+} to Ni^{2+} and Ag^{2+} to Ag^{1+}. After the injection of glucose, significant current change was obtained. The enhanced current signal may endow the NiO-Ag NFs/GCE

with higher sensitivity towards glucose detection than the NiO NFs/GCE or the porous Ag/GCE.

In addition, the dependence of peak currents on scan rates was also investigated and presented in **Fig. 11**. The redox peak currents increased linearly with the scan rate in the range from 10 to 100 mV/s (**Fig. 11b**), indicating a surface-controlled electrochemical process.

Example 10 *Amperometric detection of glucose at the NiO-Ag NFs, NiO NFs, and porous Ag modified electrodes*

The above electrocatalytic behavior study indicates that all of the three modified electrodes may have potential application in the glucose detection. In order to determine the optimum applied potential for amperometric detection of glucose, hydrodynamic voltammogram (HDV) behaviors of these three electrodes were investigated by measuring the amperometric responses to 200 μM glucose at different applied potential (-0.2 V to 0.6 V). The selection of the lowest applied potential of -0.2 V was based on the consideration of excluding the reduction of O_2; while the upper potential was chosen at 0.6 V for less interferences because higher potential is favored by interferences. **Fig. 12a** presents the HDVs of 200 μM glucose at the three different electrodes. The oxidation current of glucose at the NiO NFs/GCE was almost 0 when the detection potential was lower than 0.35 V. When the applied potential is above 0.35 V, the current rapidly increased with the increase of applied potential. Compared to the NiO NFs/GCE, porous Ag/GCE exhibited glucose oxidation signal in the potential range from -0.2 to 0.3 V with the maximum response at 0.1 V (**Fig. 12a** inset); however, there was almost no response to glucose when the applied potential was higher than 0.35 V. This phenomenon might indicate that the catalytic activity of Ag electrode is not from Ag^{1+}, and Ag^0 may be responsible for the oxidation of glucose. As for the NiO-Ag NFs/GCE, similar trend as that of porous Ag/GCE was obtained in the range from -0.2 to 0.3 V, but the response is much higher. Above 0.3 V, the hybrid nanofibers modified electrode showed the similar trend as the NiO NFs/GCE but with much higher response too, which may be attributed to the synergetic effect between NiO and Ag. The HDVs study indicated that NiO-Ag NFs not only possessed the combined performance from porous Ag and NiO NFs towards glucose oxidation, but also greatly enhanced the response.

Based on the results of HDVs, amperometric detections of glucose were carried out at 0.1 V for the porous Ag/GCE and NiO-Ag NFs/GCE (NiO NFs/GCE has no obvious response) and at 0.6 V for the NiO NFs/GCE and NiO-Ag NFs/GCE (porous Ag/GCE has no obvious

response), respectively. As shown in **Fig. 12b**, both the NiO-Ag NFs/GCE and the porous Ag/GCE rapidly response to the addition of glucose at 0.1 V, achieving 95% of steady-state current within 5 s and 6 s, respectively, which is even faster than enzyme-based glucose sensor. The sensitivity of the NiO-Ag NFs/GCE to glucose at 0.1 V was ~55 folds higher than that obtained at the porous Ag/GCE. On the other hand, at an applied potential of 0.6 V, the NiO-Ag NFs/GCE also showed 5.2-fold higher sensitivity, lower detection limit and wider linear range than the NiO NFs/GCE (**Fig. 12c**). Both the sensitivity and detection limit obtained at the NiO-Ag nanofibers modified electrode at 0.6 V are among the best reported values for non-enzymatic glucose sensors. The analytical characteristics of different electrodes at different applied potentials were summarized in **Table 2**. The significant improvements obtained with NiO-Ag NFs may be attributed to the use of abundant nanofibers which can provide numerous electron transfer tunnels, the highly porous structure which can minimize the diffusion resistance of analytes, and the synergetic effect between NiO and Ag.

Table 2. Analytical characteristics of different electrodes at an applied potential of 0.1 V or 0.6 V

	NiO-Ag NFs/GCE at 0.1 V	**Porous Ag/GCE at 0.1 V**	**NiO-Ag NFs/GCE at 0.6 V**	**NiO NFs/GCE at 0.6 V**
Linear range up to / mM	0.59 (R = 0.991)	0.48 (R = 0.991)	2.63 (R = 0.993)	1.94 (R = 0.993)
Detection limit / μM	1.37	7.99	0.72	1.28
Sensitivity / μA mM^{-1} cm^{-2}	19.3	0.35	170.2	32.91

Example 11 *Anti-interference property, reproducibility study and real sample detection*

Good selectivity is very important but challenging aspect to non-enzymatic glucose sensor since the easily oxidative species such as ascorbic acid (AA) and uric acid (UA) usually co-exist with glucose in human blood and non-enzymatic glucose sensor is generally lack of such selectivity. The blood glucose level of a normal human body is between 4 and 7 mM, while the concentration of endogenous AA and UA is about 0.125 mM and 0.33 mM in blood samples, respectively. As presented in **Fig. 13a**, the response of the porous Ag/GCE to 0.125 mM AA and 0.33 mM UA are 17-fold and 55-fold higher than that of 4 mM glucose at

0.1 V. This may be explained by the catalytic activity of porous Ag towards AA and UA oxidation. In contrast, at 0.1 V, the response of NiO-Ag NFs/GCE to AA and UA was only 33% and 40% of glucose response, respectively. The improved selectivity against UA and AA at the NiO-Ag NFs/GCE can be hypothesized as the repelling effect described in **Fig. 14**. NiO has an isoelectic point (IEP) of 10-11, which means in 0.1 M NaOH solution (pH=13), the surface of NiO nanofibers would be negatively charged. UA and AA are also negatively charged in 0.1 M NaOH solution due to the loss of proton. Consequently, the negatively charged NiO-Ag nanofibers surface could strongly repel the negatively charged UA and AA molecules, thus reducing the electrooxidation of UA and AA on the surface of NiO-Ag nanofibers and resulting in an improved selectivity. This explanation is also valid at the applied potential of +0.6 V, at which the NiO-Ag NFs/GCE and NiO NFs/GCE show excellent selectivity against AA and UA. 0.125 mM AA only induces 1.98% current increase in the 4 mM glucose detection at the NiO NFs/GCE and 4.11% increase at the NiO-Ag NFs/GCE, while 0.33 mM UA only induce 5.01% increase at the NiO NFs/GCE and 6.13% increase at the NiO-Ag NFs/GCE (**Fig. 13b**). Besides the repelling effect, another factor attributing to such superior selectivity at 0.6 V (compared to at 0.1 V) may be stronger enhancement for glucose oxidation than for UA and AA oxidation at the NiO-Ag NFs and NiO NFs.

Reproducibility of NiO-Ag nanofibers modified electrode was also investigated at 0.6 V. The relative standard deviation (R.S.D) of 7.73% (n = 8) for 200 μM glucose demonstrated good intra-electrode reproducibility. In addition, the good inter-electrode reproducibility was characterized by the low R.S.D of 6.64% in the response to 200 μM glucose on five NiO-Ag NFs/GCEs.

The as-prepared NiO-Ag nanofibers based non-enzymatic glucose sensor was further applied to the detection of glucose in human blood serum sample at an applied potential of 0.6 V. **Fig. 15** demonstrated the amperometric response to successive additions of analytes (standard glucose solution, human serum sample, AA, and UA). The concentration of glucose in serum sample was calibrated using standard glucose solution and compared with the result obtained by commercial GOx-based glucose meter (OneTouch UltraMini, Life Scan, Inc, CA). As presented in **Table 3**, the good agreement between the results obtained by our sensor and that read from the commercial GOx-based glucose meter indicates the potential practical application of the as-prepared non-enzymatic glucose sensor. In addition, the injection of 10 μL 0.125 mM AA, and 10 μL 0.33mM UA into 5 mL testing electrolyte would not cause any measurable signal and also not affect the detection of glucose in serum sample (**Fig. 15**).

Furthermore, the low cost of the as-prepared materials and the inherent stability of the inorganic materials make the developed non-enzymatic sensor very appealing.

Table 3. The glucose concentration in human blood serum sample measured by a commercial glucose meter and our NiO-Ag NFs based sensor

	Commercial glucose meter (mM)	Our sensor (mM)
Reading	11.68±0.363	12.05±0.305

NiO-Ag hybrid nanofibers (average dia. 82.1 nm), NiO nanofibers (average dia. 72.6 nm), and porous Ag were prepared by calcination of electrospun $Ni(NO_3)_2$-$AgNO_3$-PVP nanofibers, $Ni(NO_3)_2$-PVP nanofibers, and $AgNO_3$-PVP nanofibers, respectively. FTIR was used to confirm the degradation of PVP and the complete decomposition of metal salts. XRD and XPS were performed to investigate the crystalline structure and compositions of the calcined products. SEM and TEM were employed to compare the morphology before and after calcination. The as-prepared NiO-Ag nanofibers, NiO nanofibers, and porous Ag were applied in the non-enzymatic glucose detection and a comparative study was conducted. A synergistic effect was obtained between NiO and Ag, endowing NiO-Ag nanofibers modified electrode with higher sensitivity, lower detection limit and wider linear range compared to NiO nanofibers and porous Ag modified electrodes. In addition, at an applied potential of 0.6 V, the NiO-Ag nanofibers and NiO nanofibers based sensors have an excellent anti-interference property towards the electroactive compounds such as AA and UA. The real sample detection was also conducted with the human blood serum, and the good agreement between the results obtained by our NiO-Ag nanofibers-based non-enzymatic glucose sensor and the commercial GOx-based glucose meter indicated potential practical application of our sensor in glucose detection.

While the invention has been described with reference to preferred embodiments, it will be understood by those skilled in the art that various changes may be made and equivalents may be substituted for the elements thereof without departing from the scope of the invention. In addition, many modifications may be made to adapt the teaching of the invention to particular use, application, manufacturing conditions, use conditions, composition, medium, size, and/or materials without departing from the essential scope thereof. Therefore, it is intended that the invention not be limited to the particular

embodiments and best mode contemplated for carrying out this invention as described herein. The accompanying claims are intended to cover such modifications as would fall within the true scope and spirit of the present invention.

WE CLAIM:

1. A non-enzymatic glucose sensor comprising an electrode, one or more metal oxide nanofibers, and an alkaline solid electrolyte, wherein
   the metal oxide nanofibers and an alkaline solid electrolyte are each disposed over a surface of the electrode,
   at least a portion of the alkaline solid electrolyte is in contact with the metal oxide nanofibers, and
   the metal oxide nanofibers are each independently and optionally metal doped.

2. The non-enzymatic glucose sensor of claim 1 wherein the metal oxide nanofibers comprise Co_3O_4, NiO, CuO, or a mixture thereof.

3. The non-enzymatic glucose sensor of claim 1 wherein the metal oxide nanofibers comprise two or more metal oxides selected from the group consisting of Co_3O_4, NiO, CuO, ZnO, SnO_2, CeO_2, MnO_2, RuO_2, and CdO.

4. The non-enzymatic glucose sensor of any one of claims 1- 3, wherein the metal oxide nanofibers are metal-doped metal oxide nanofibers.

5. The non-enzymatic glucose sensor of claim 4, wherein the metal-doped metal oxide nanofibers comprise one or more doping metals selected from ruthenium, rhodium, palladium, silver, osmium, iridium, platinum, gold, and mixtures thereof.

6. The non-enzymatic glucose sensor of any one of claims 1 – 5, wherein the metal oxide nanofibers or metal-doped metal oxide nanofibers comprise Co_3O_4 or NiO.

7. The non-enzymatic glucose sensor of any one of claims 1 - 6, wherein the alkaline solid electrolyte is a sulfonated tetrafluoroethylene polymer, sodium hydroxide, or potassium hydroxide.

8. The non-enzymatic glucose sensor of claim 7, wherein the alkaline solid electrolyte is nanoporous.

9. The non-enzymatic glucose sensor of claim 1, wherein the metal oxide nanofibers comprise NiO-Ag nanofibers.

10. The non-enzymatic glucose sensor of claim 1, wherein the metal oxide nanofibers comprise NiO-Ag nanofibers, Co_3O_4-Ag nanofibers, CuO-Ag nanofibers, or a combination thereof.

11. The non-enzymatic glucose sensor of any one of claims 1 – 10, wherein the electrode is a gold, silver, platinum, copper, glassy carbon, or pyrolytic carbon electrode.

12. A glucose detection apparatus comprising a non-enzymatic glucose sensor of any one of claims 1 to 11.

13. The glucose detection apparatus of claim 12, further comprising a temperature sensor positioned to detect the temperature at or near a surface of the non-enzymatic glucose sensor.

14. The glucose detection apparatus of claim 13, further comprising programmed software to calibrate for a temperature effect on performance of the non-enzymatic glucose sensor.

15. A method for preparing a non-enzymatic glucose sensor comprising,
depositing one or more metal oxide nanofibers and an alkaline solid electrolyte on an electrode surface, wherein the metal oxide nanofibers are optionally metal doped.

16. The method of claim 15, wherein the depositing is depositing one or more metal oxide nanofibers on the electrode surface, and depositing an alkaline solid electrolyte over the metal oxide nanofibers.

17. The method of claim 15, wherein the depositing is co-depositing the optionally metal doped metal oxide nanofibers and the alkaline solid electrolyte on the electrode surface.

18. The method of claim 17, wherein the optionally metal-doped metal oxide nanofibers are prepared by electrospinning a solution comprising at least one metal oxide precursor, one or more optional metal precursors, and a polymer to yield polymer composite fibers and calcining the polymer composite fibers.

19. A glucose test strip comprising a support material comprising a working electrode wherein the working electrode comprises a surface coating comprising one or more metal oxide nanofibers and an alkaline solid electrolyte, and wherein the metal oxide nanofibers are optionally metal-doped.

20. The glucose test strip of claim 19, further comprising a counter electrode and a reference electrode, each positioned in electrochemical communication with the working electrode.

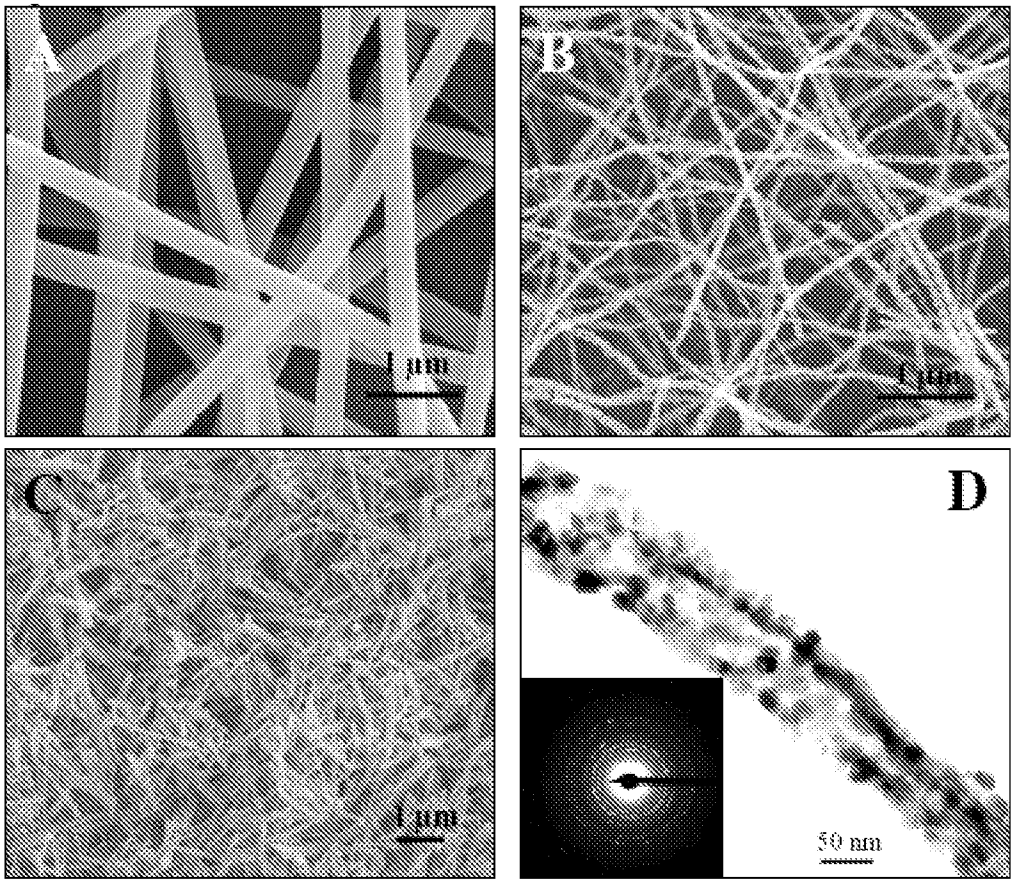

Figure 1

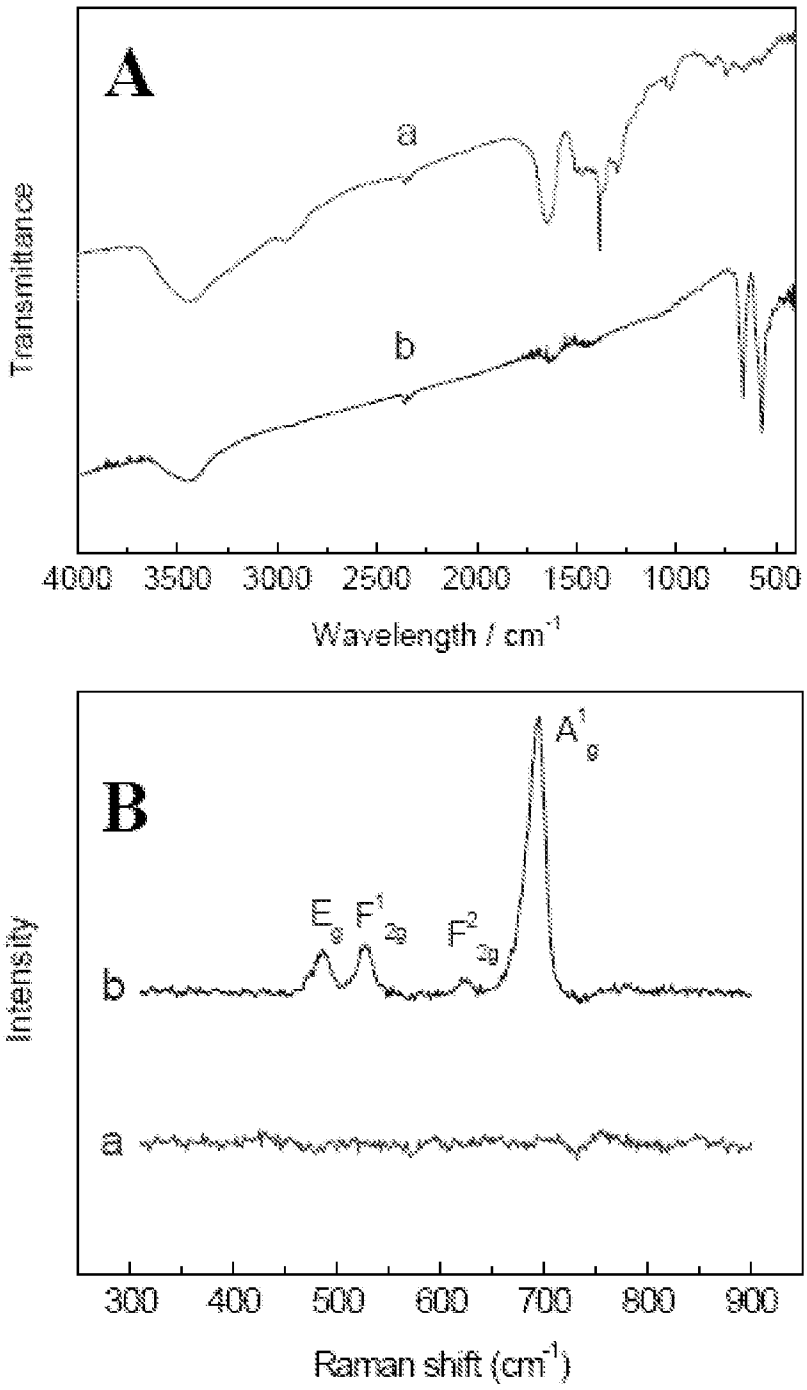
A
a
b
Transmittance
4000 3500 3000 2500 2000 1500 1000 500
Wavelength / cm-1
B
A1g
E2g
F1 2g
F2 2g
b
a
Intensity
300 400 500 600 700 800 900
Raman shift (cm-1)

Figure 2

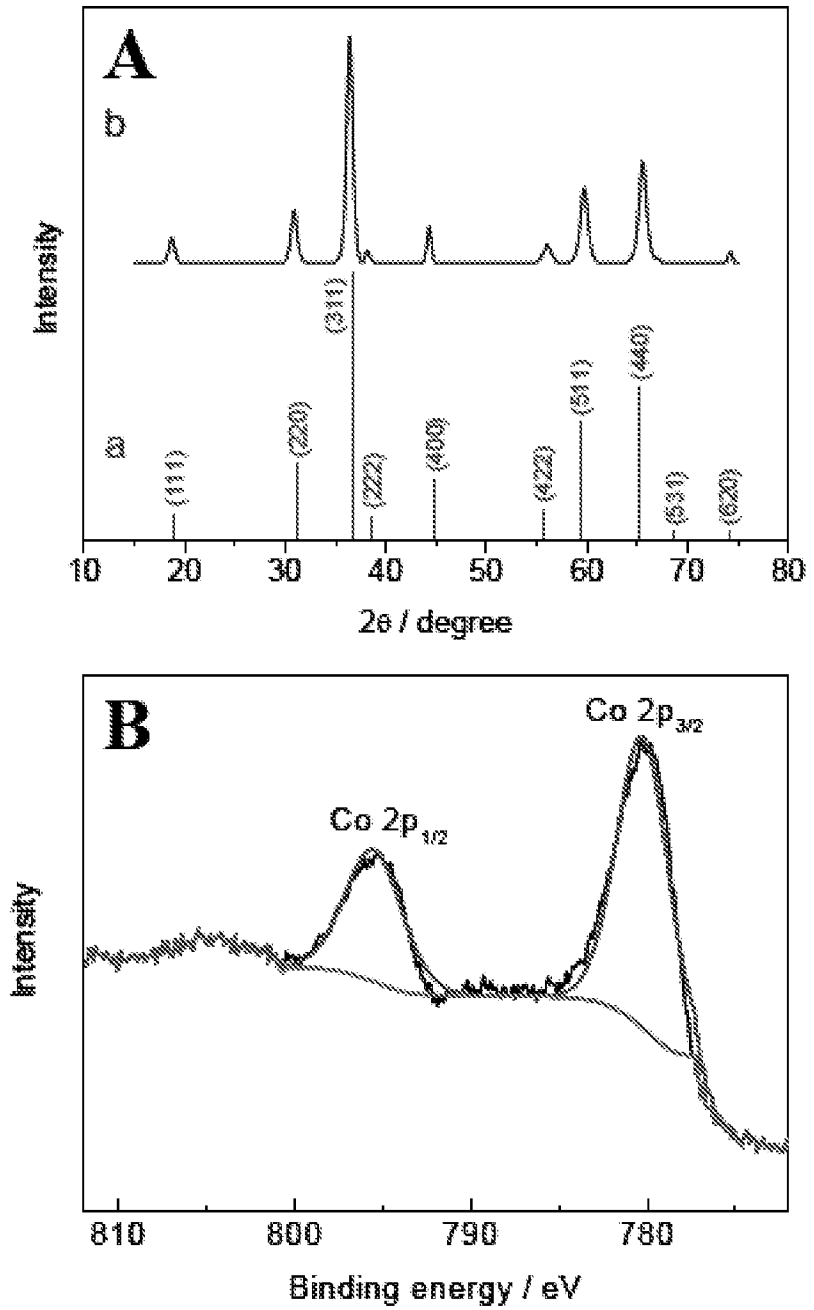
A
b
a
Intensity
(111)
(220)
(311)
(222)
(400)
(422)
(511)
(440)
(531)
(620)
10
20
30
40
50
60
70
80
2θ / degree
B
Co 2p3/2
Co 2p1/2
Intensity
810
800
790
780
Binding energy / eV

Figure 3

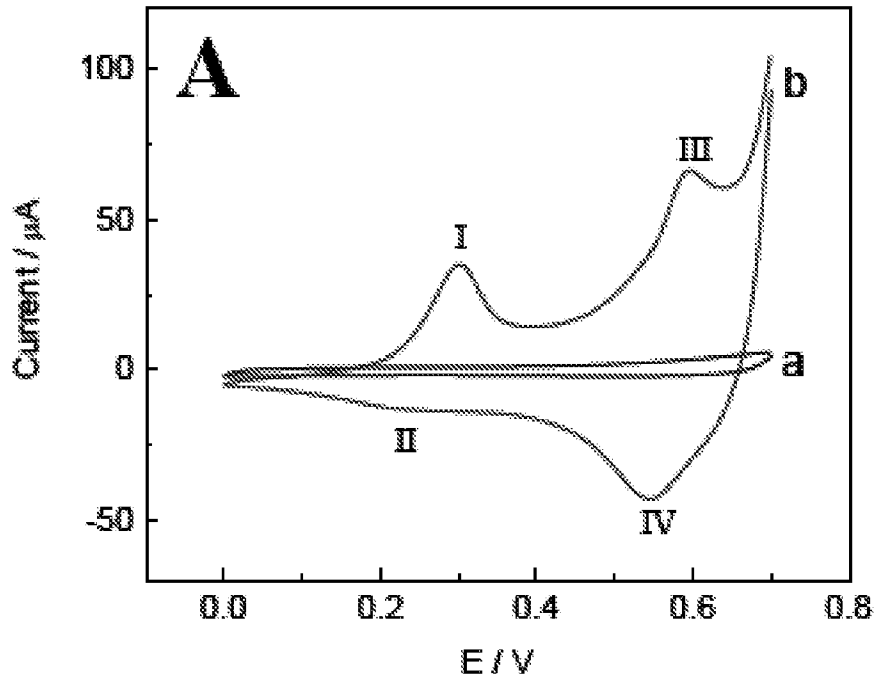

Figure 4a

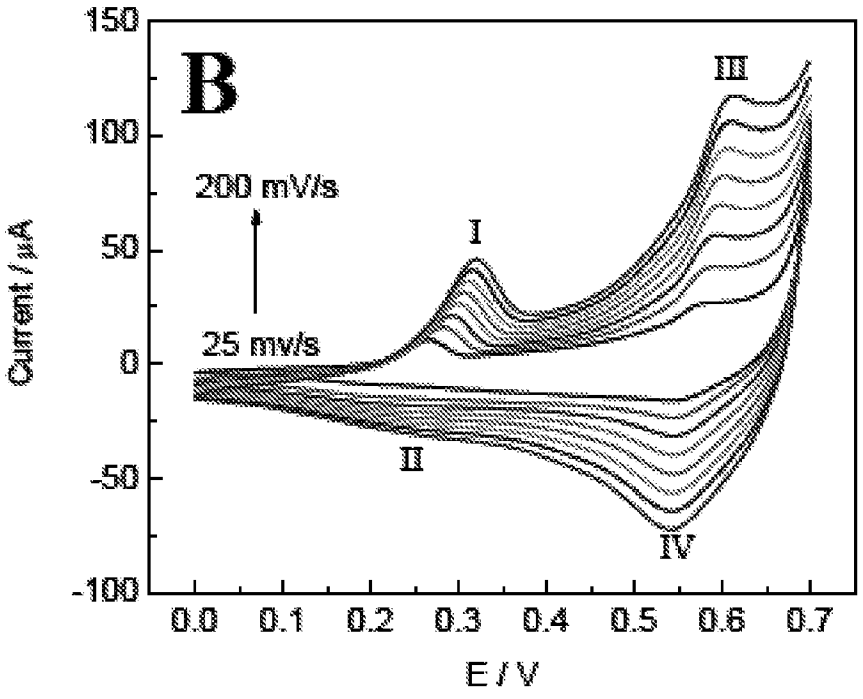

Figure 4b

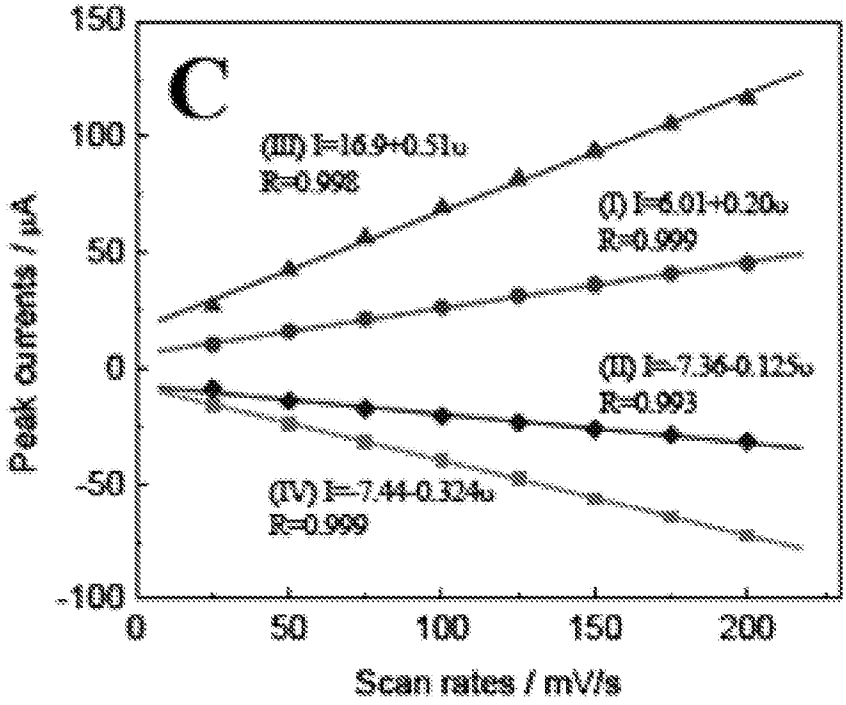
C
(III) I=16.9+0.51υ
R=0.998
(I) I=6.01+0.20υ
R=0.999
(II) I=-7.36-0.125υ
R=0.993
(IV) I=-7.44-0.324υ
R=0.999
Peak currents / μA
Scan rates / mV/s
150
100
50
0
-50
-100
0
50
100
150
200

Figure 4c

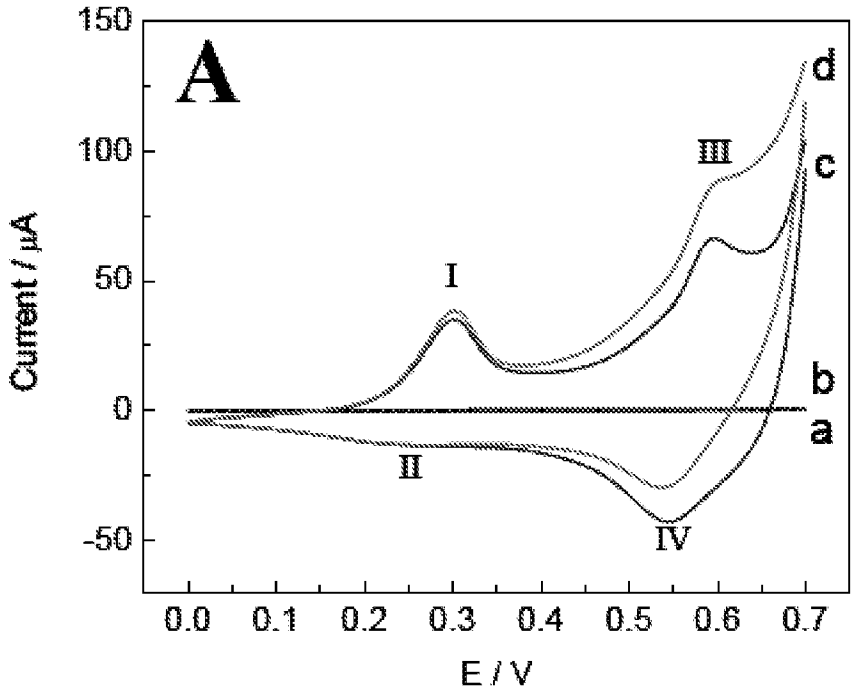

Figure 5a

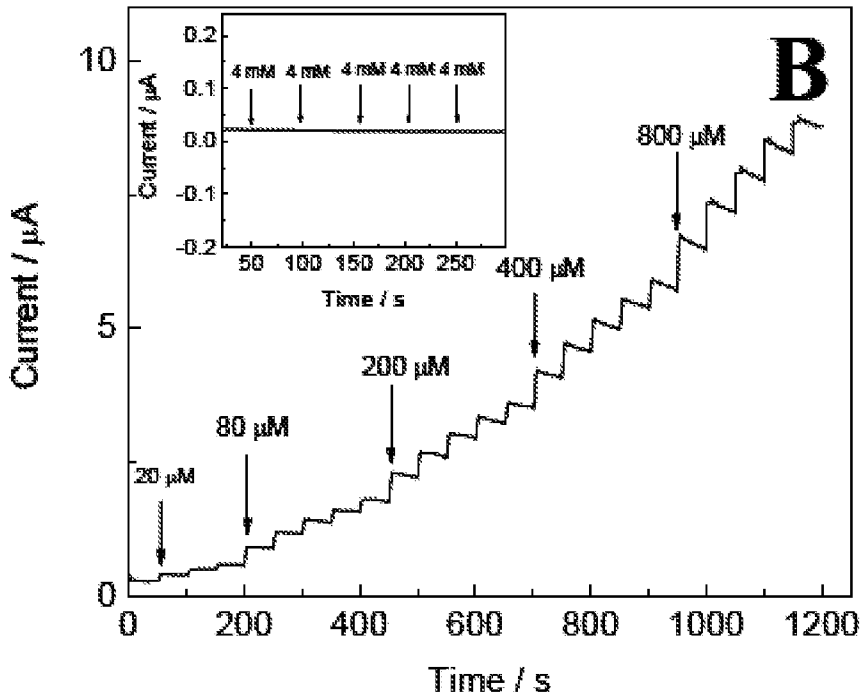

Figure 5b

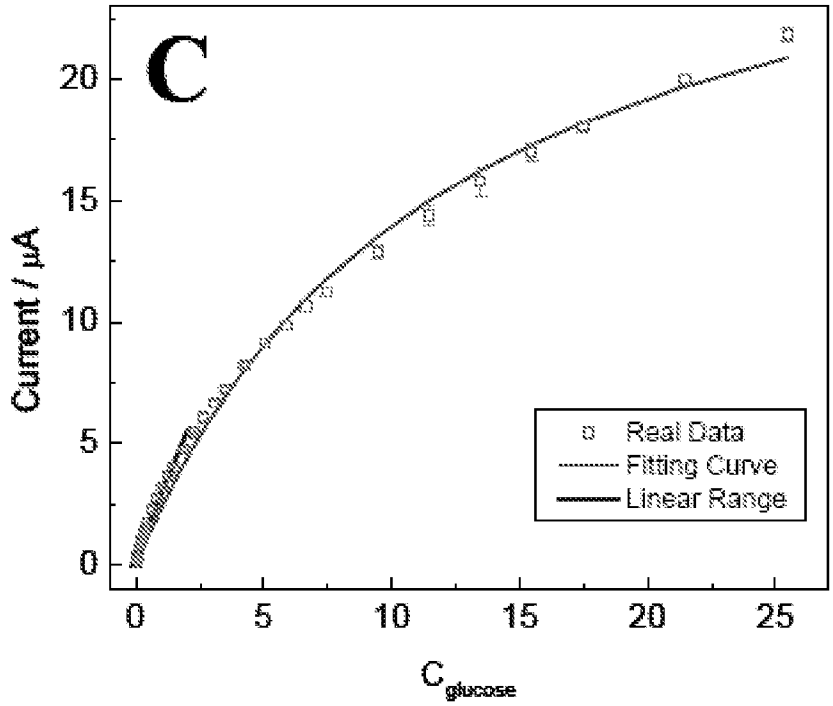

Figure 5c

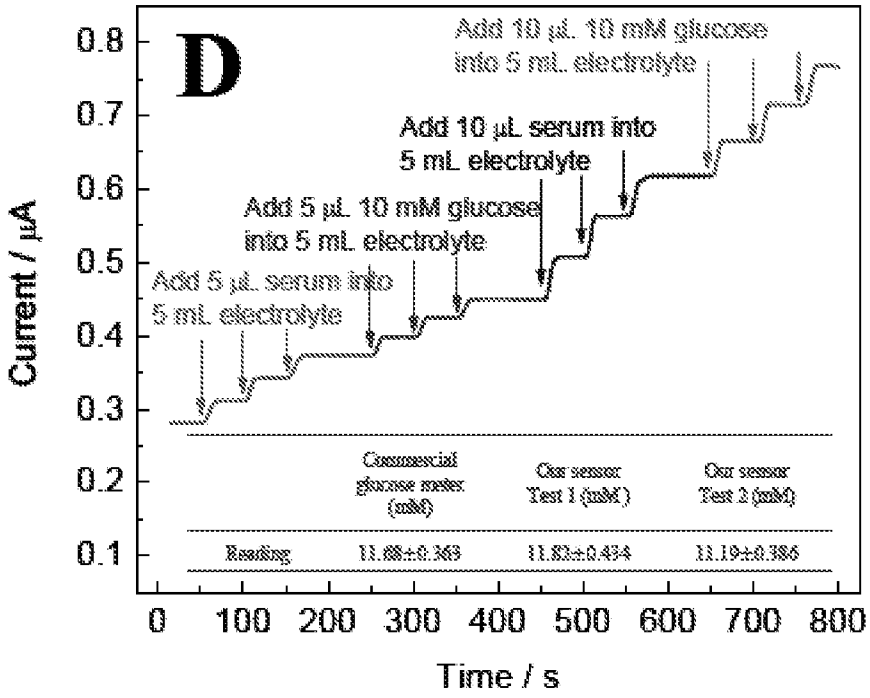

Figure 5d

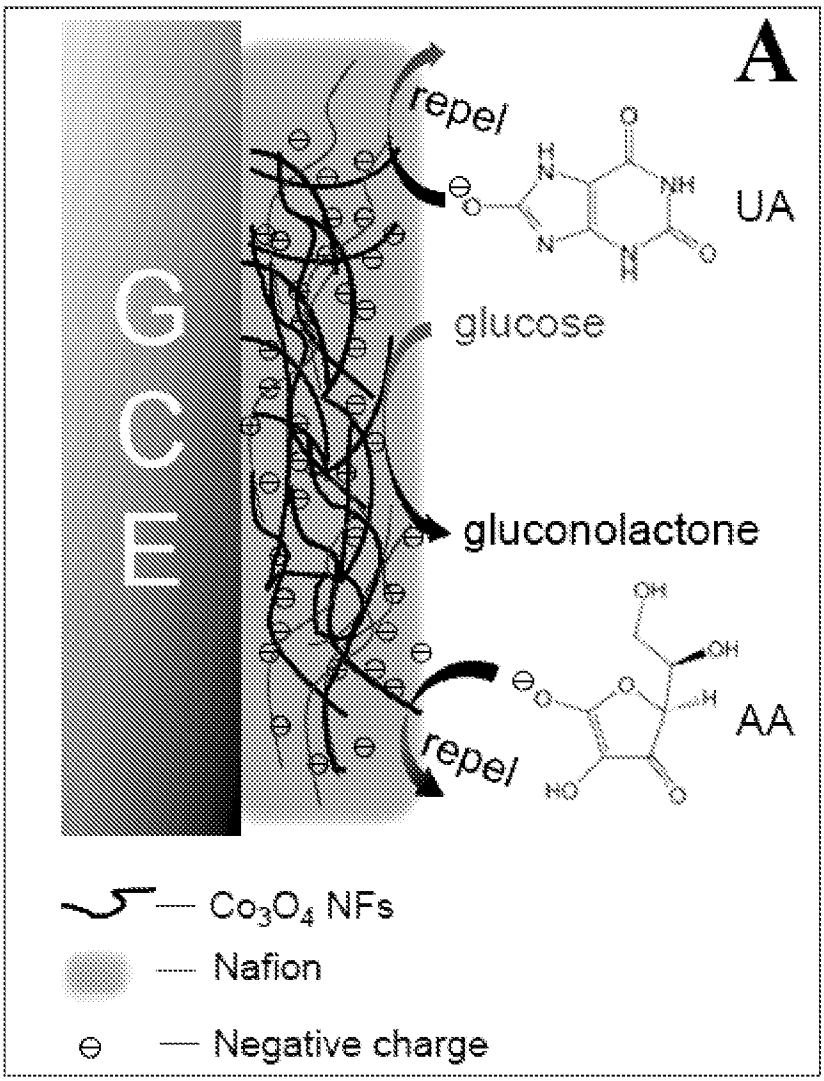
A
repel
UA
glucose
GCE
gluconolactone
AA
repel
Co_3O_4 NFs
Nafion
Negative charge

Figure 6

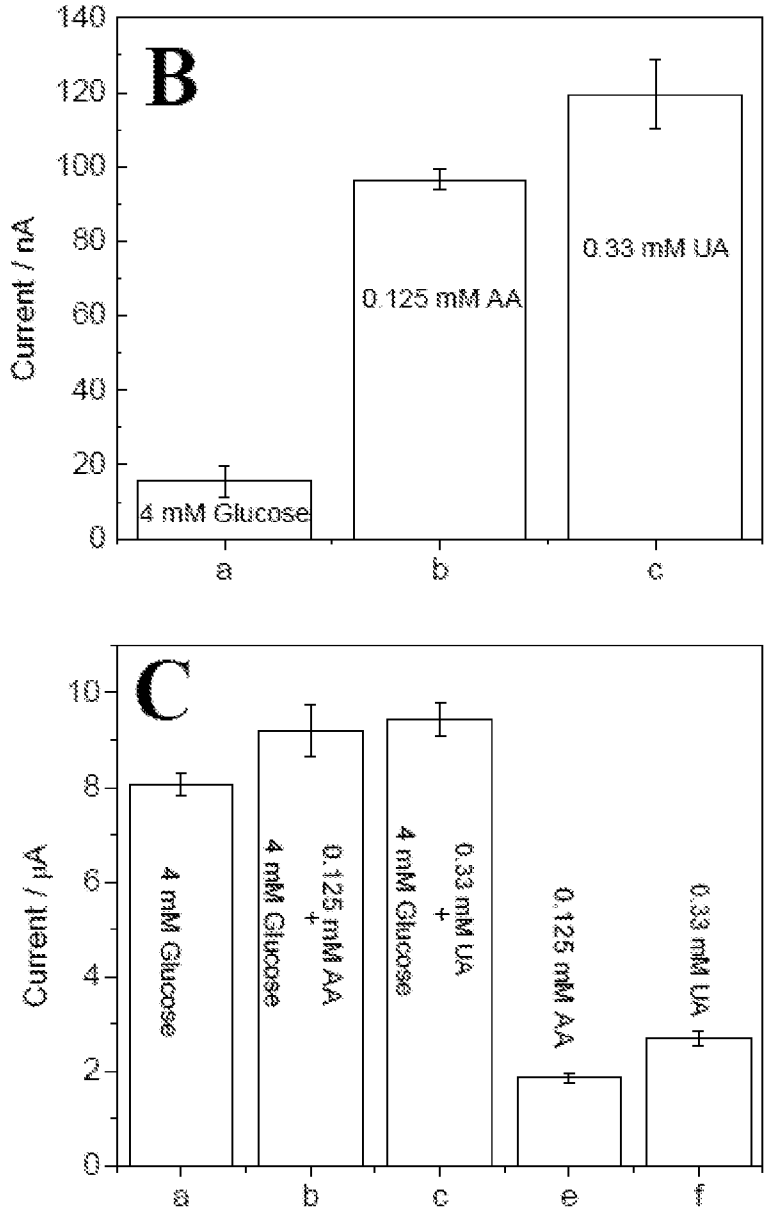

Figure 6 cont'd

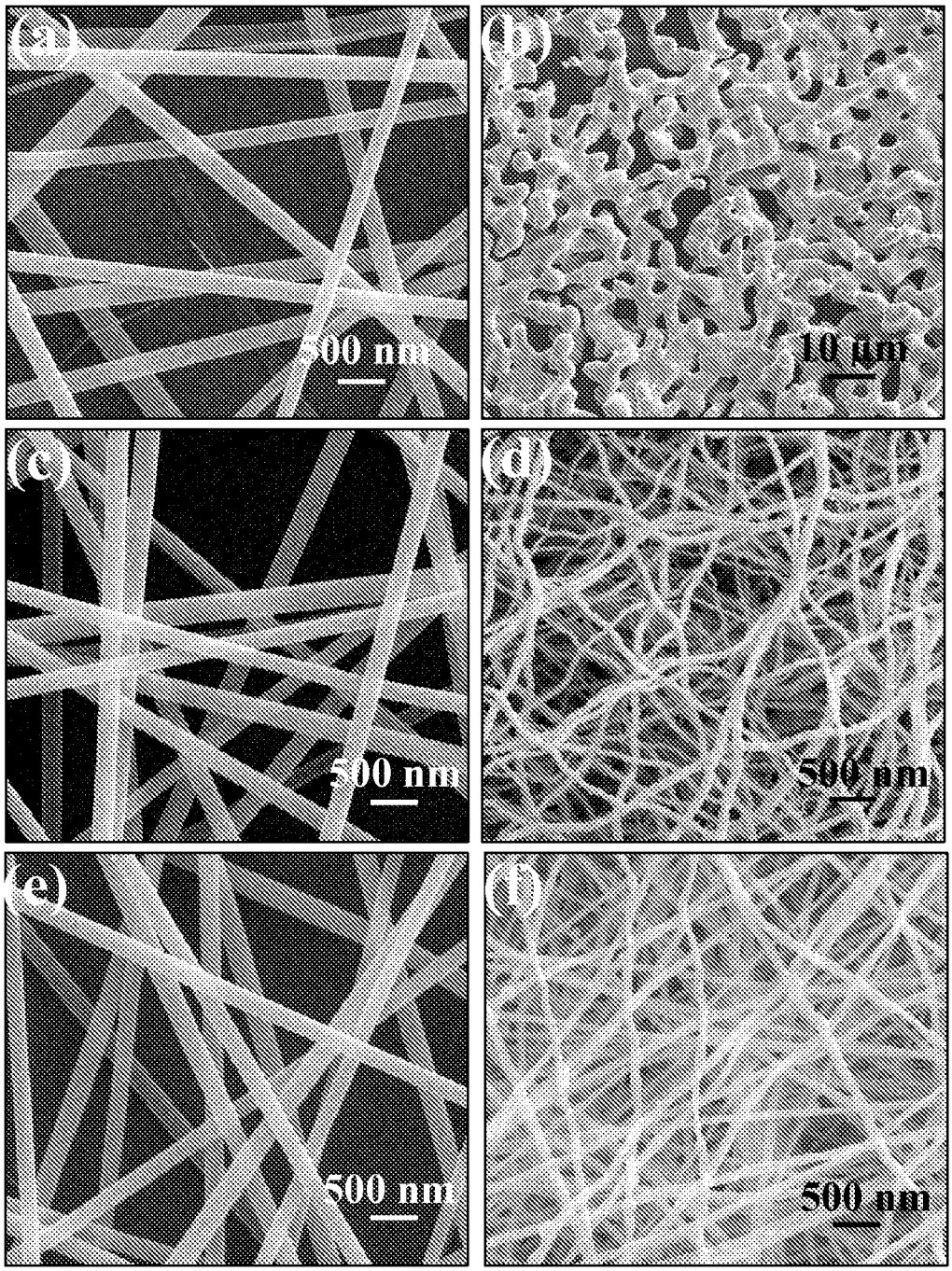

Figure 7

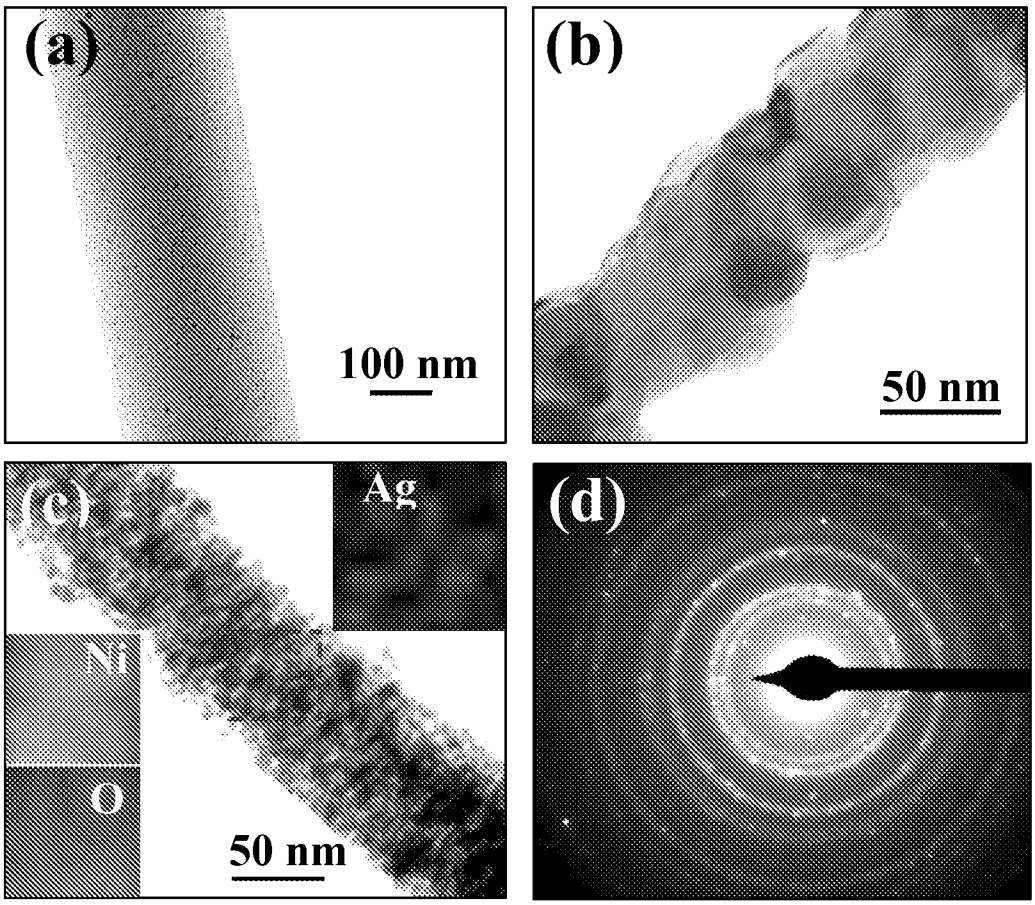

Figure 8

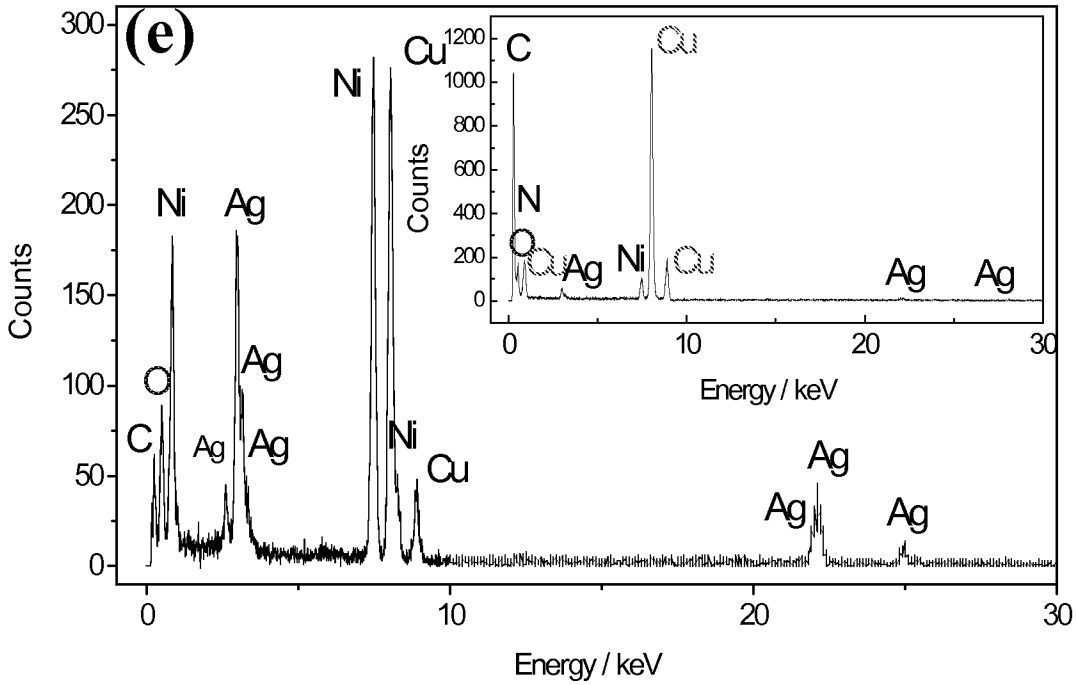
(e)
Counts
Energy / keV
C
O
Ni
Ag
Cu
N
Ag
Ag
Ag
Ag
Ag
Ag
Ni
Cu
Ni
Ag
Ag
Ag
Ag
Ag
Ag

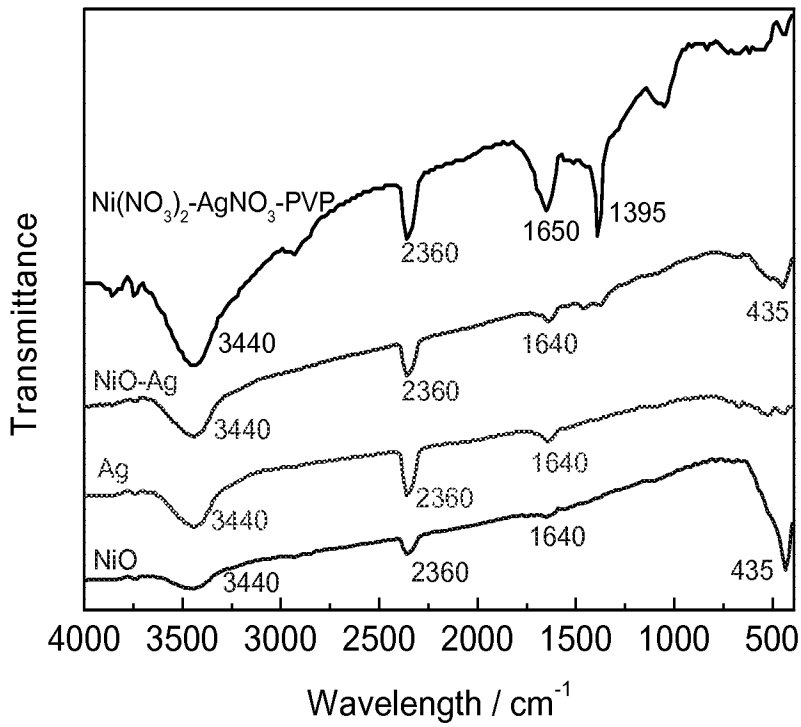

Figure 9a

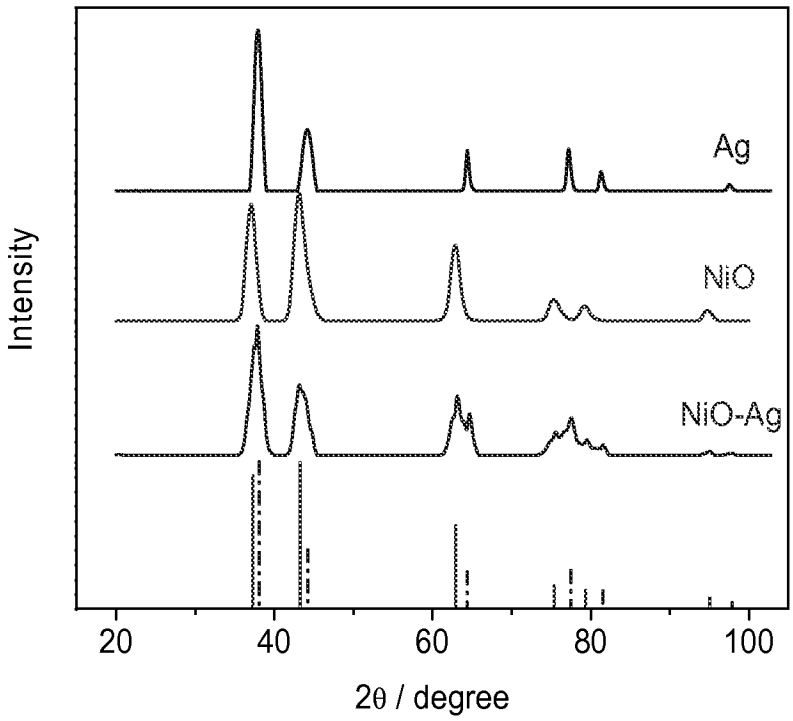

Figure 9b

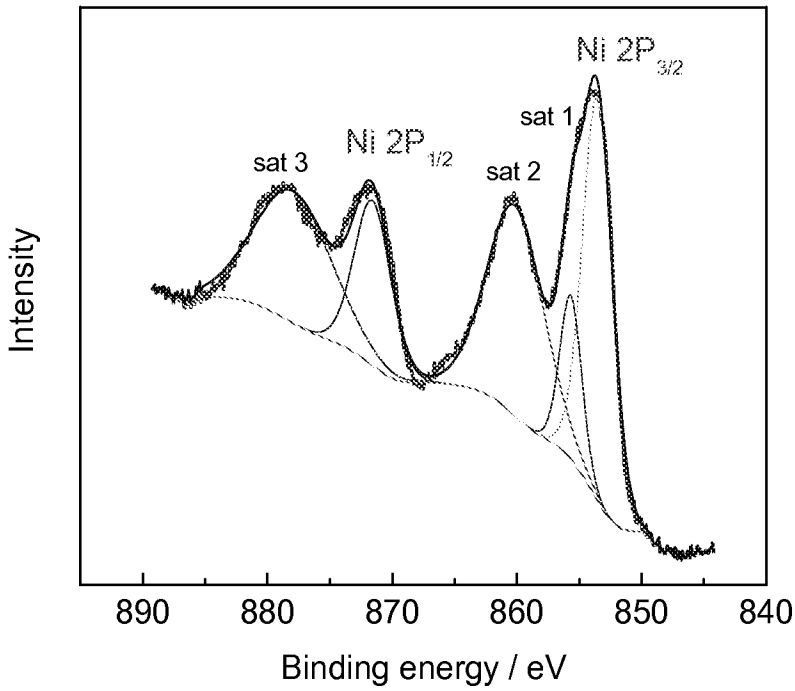

Figure 9c

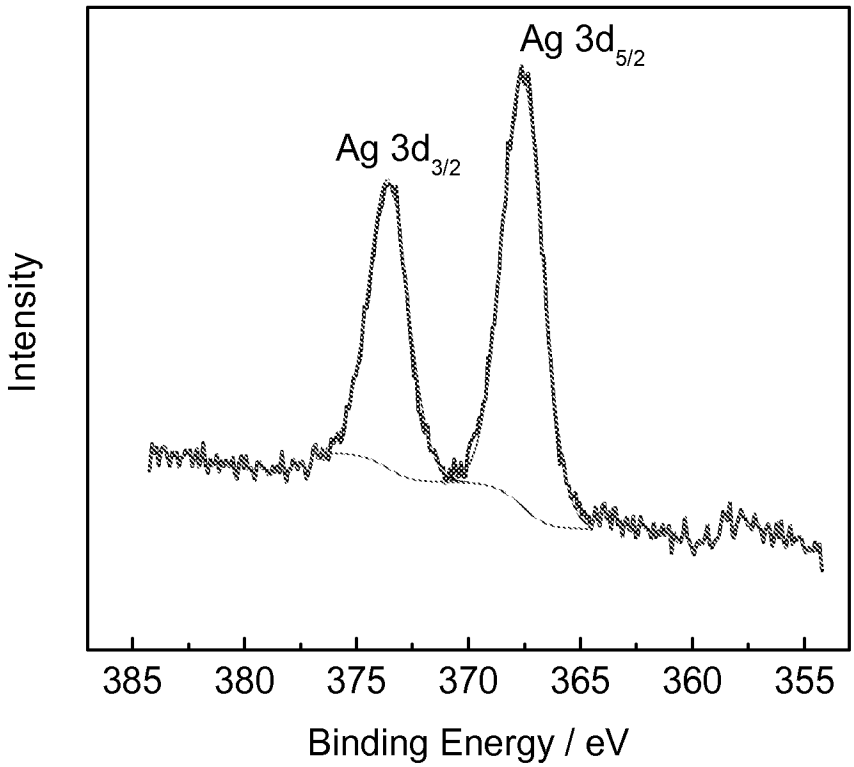

Figure 9d

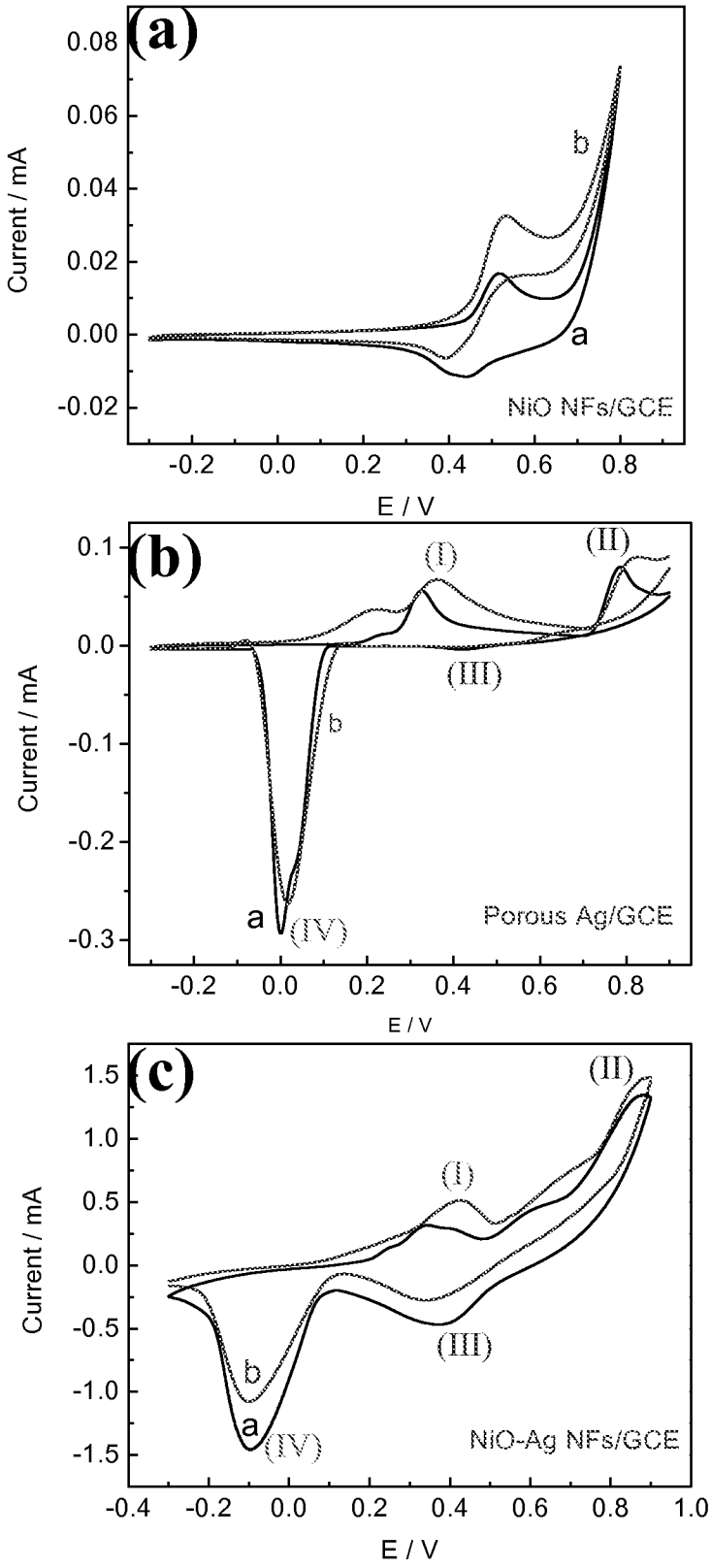
(a)
Current / mA
E / V
b
a
NiO NFs/GCE
(b)
(I)
(II)
(III)
(IV)
b
a
Porous Ag/GCE
(c)
(I)
(II)
(III)
(IV)
b
a
NiO-Ag NFs/GCE

Figure 10

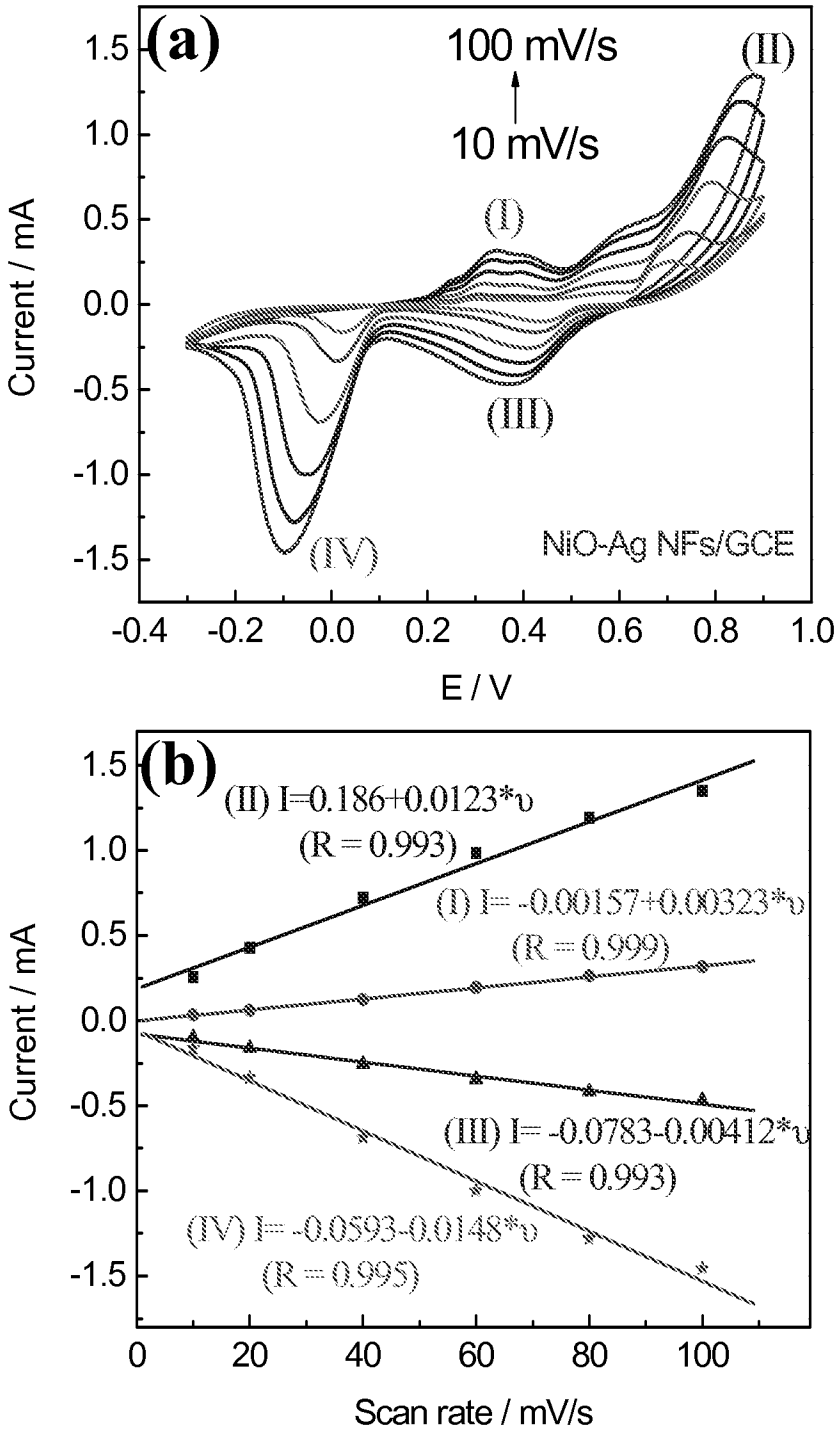
(a)
100 mV/s
10 mV/s
(I)
(II)
(III)
(IV)
NiO-Ag NFs/GCE
Current / mA
E / V
(b)
(II) I=0.186+0.0123*υ
(R = 0.993)
(I) I= -0.00157+0.00323*υ
(R = 0.999)
(III) I= -0.0783-0.00412*υ
(R = 0.993)
(IV) I= -0.0593-0.0148*υ
(R = 0.995)
Current / mA
Scan rate / mV/s

Figure 11

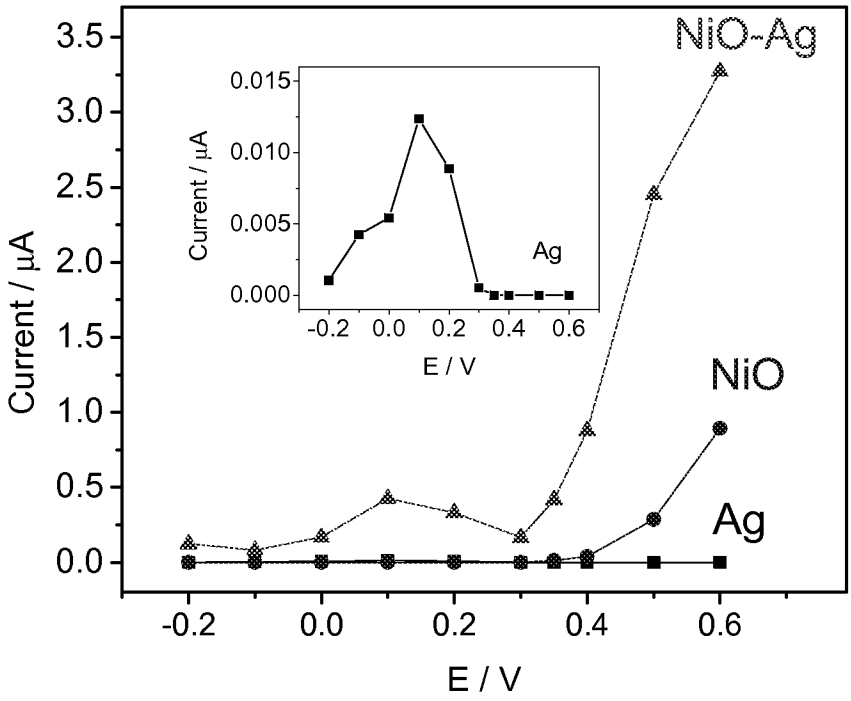

Figure 12a

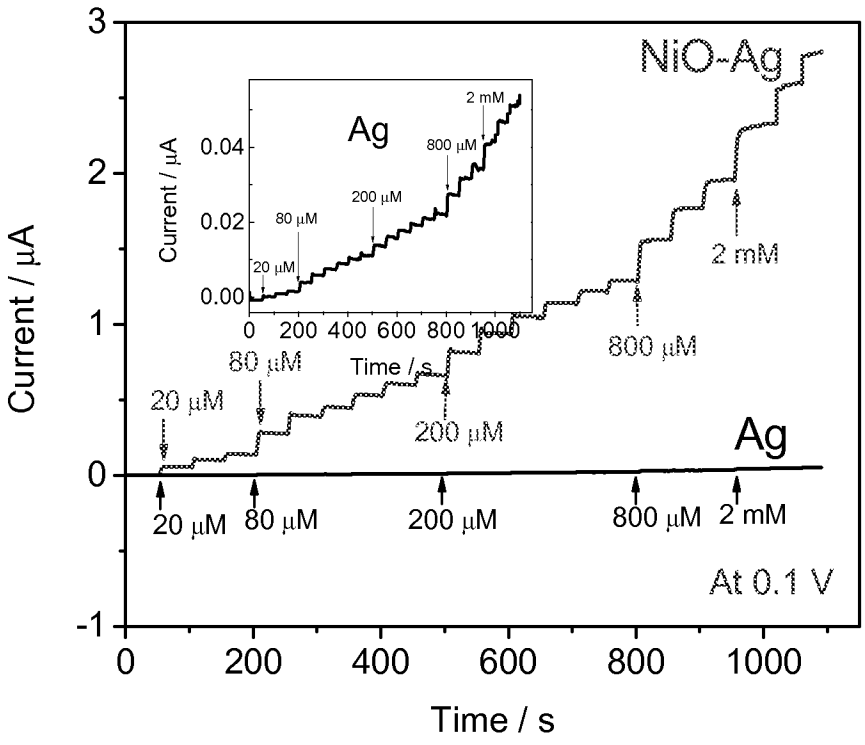

Figure 12b

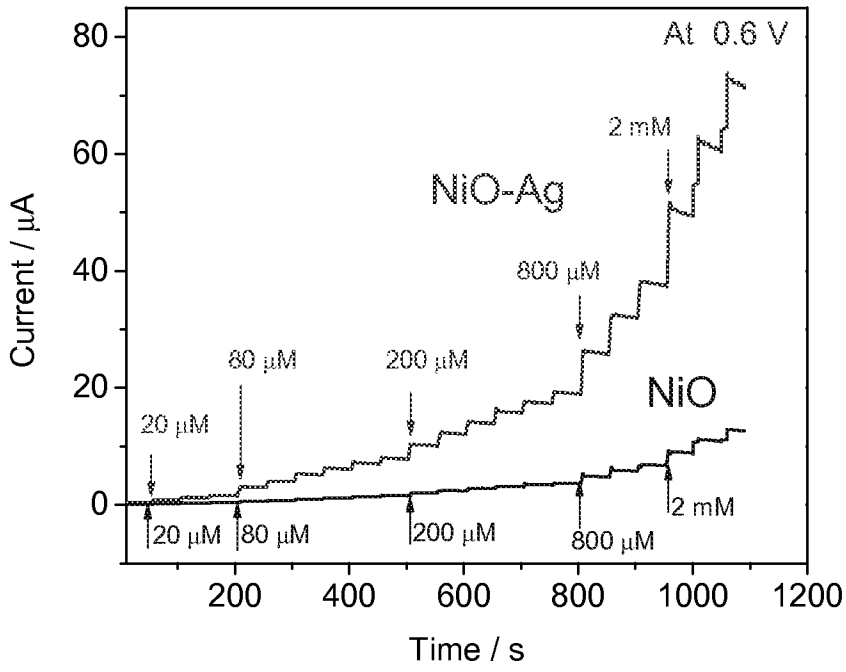

Figure 12c

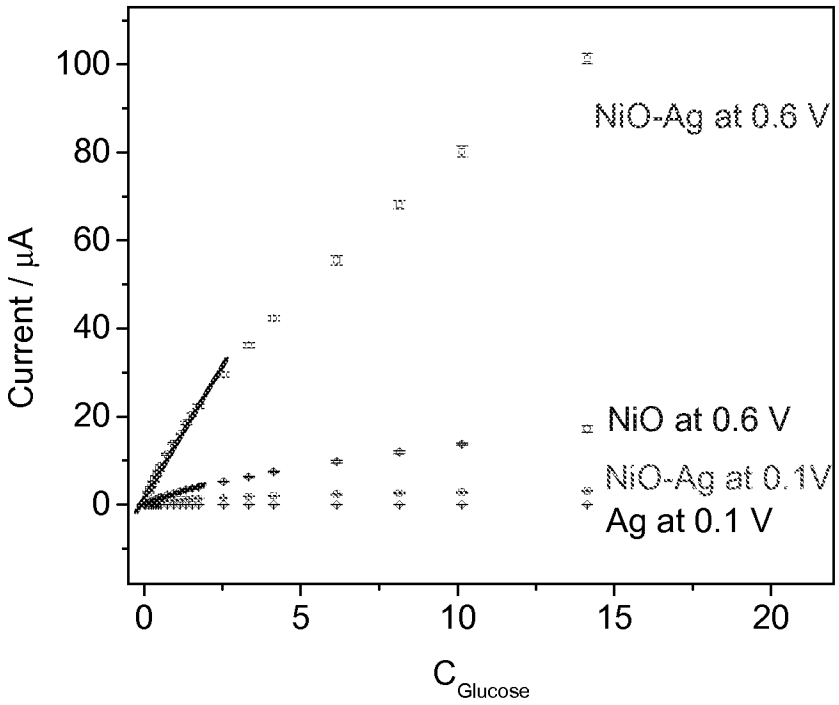

Figure 12d

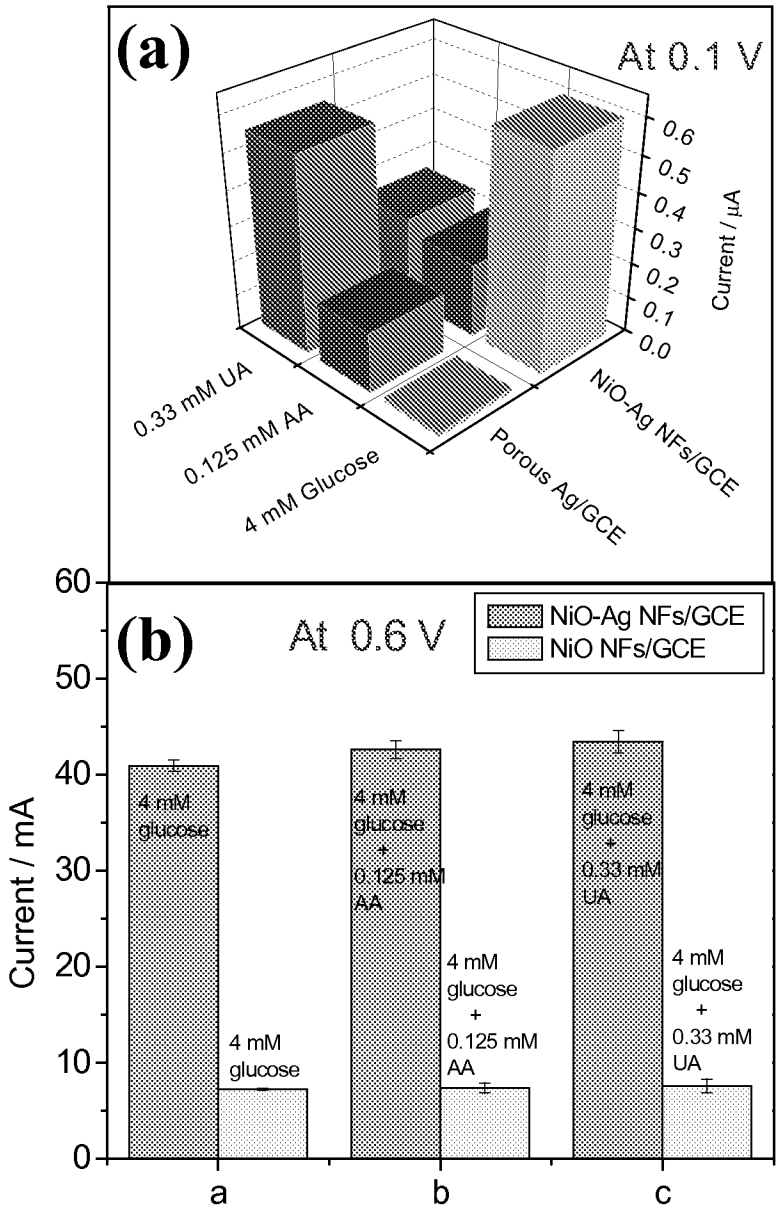
(a)
At 0.1 V
0.6
0.5
0.4
0.3
0.2
0.1
0.0
Current / μA
0.33 mM UA
0.125 mM AA
4 mM Glucose
Porous Ag/GCE
NiO-Ag NFs/GCE
(b)
At 0.6 V
NiO-Ag NFs/GCE
NiO NFs/GCE
Current / mA
60
50
40
30
20
10
0
4 mM glucose
4 mM glucose
4 mM glucose + 0.125 mM AA
4 mM glucose + 0.125 mM AA
4 mM glucose + 0.33 mM UA
4 mM glucose + 0.33 mM UA
a
b
c

Figure 13

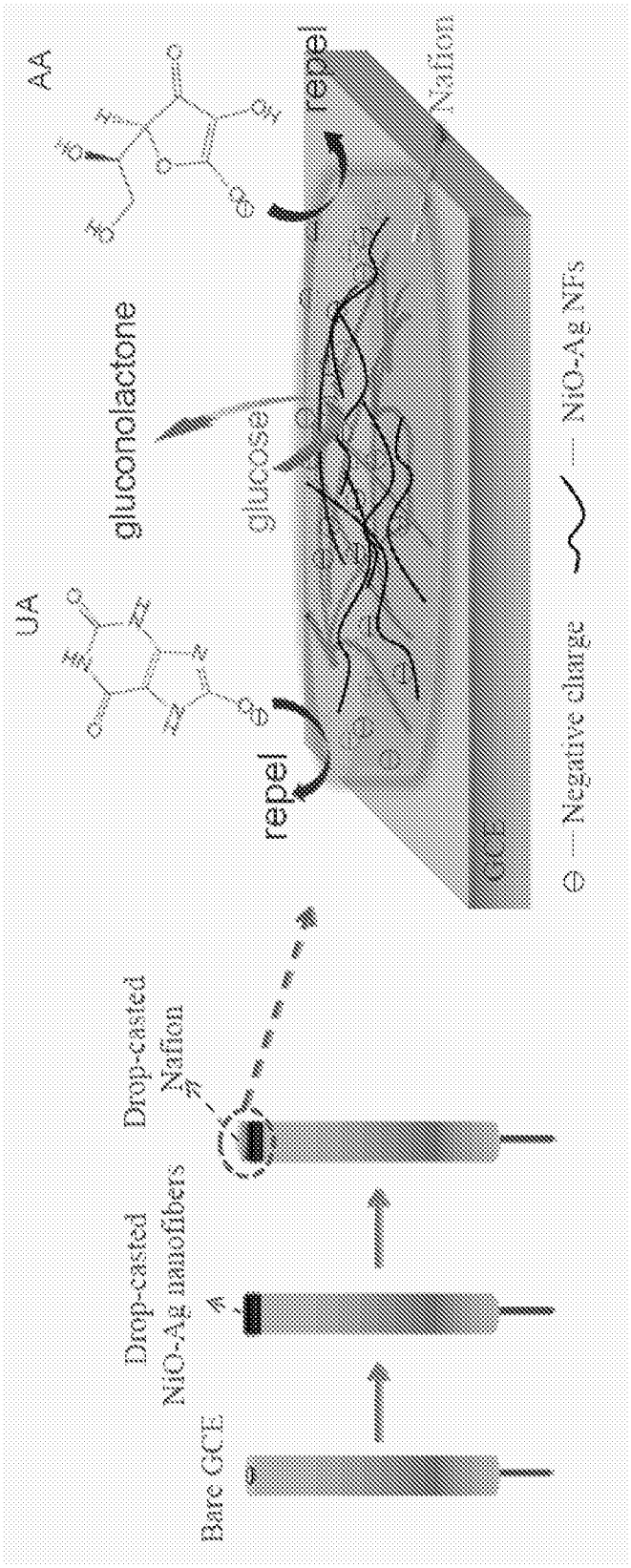
AA
UA
gluconolactone
glucose
repel
repel
Nafion
⊖ — Negative charge
— NiO-Ag NFs
Drop-casted
NiO-Ag nanofibers
Drop-casted
Nafion
Bare GCE

Figure 14

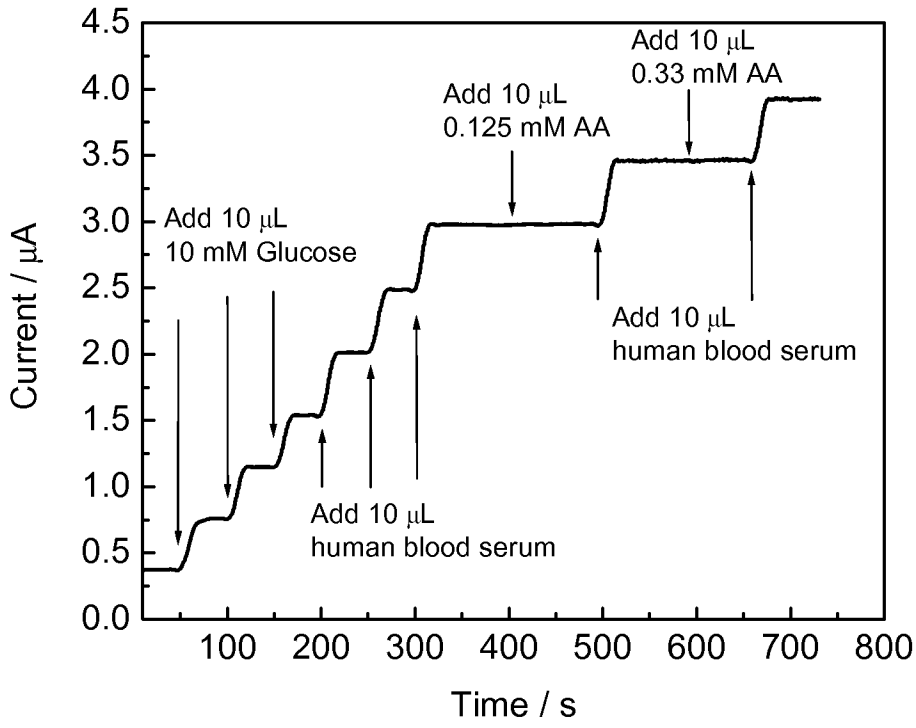
Current / μA
Time / s
Add 10 μL
10 mM Glucose
Add 10 μL
human blood serum
Add 10 μL
0.125 mM AA
Add 10 μL
human blood serum
Add 10 μL
0.33 mM AA

Figure 15

INTERNATIONAL SEARCH REPORT

International application No
PCT/US2011/046214

A. CLASSIFICATION OF SUBJECT MATTER
INV. B82Y15/00 B82Y30/00 A61B5/145 G01N33/487
ADD.

According to International Patent Classification (IPC) or to both national classification and IPC

B. FIELDS SEARCHED

Minimum documentation searched (classification system followed by classification symbols)
B82Y A61B G01N

Documentation searched other than minimum documentation to the extent that such documents are included in the fields searched

Electronic data base consulted during the international search (name of data base and, where practical, search terms used)
EPO-Internal

C. DOCUMENTS CONSIDERED TO BE RELEVANT

Category*	Citation of document, with indication, where appropriate, of the relevant passages	Relevant to claim No.
X	GUANGFENG WANG ET AL: "Enzyme-free amperometric sensing of glucose using Cu-CuO nanowire composites", MICROCHIMICA ACTA ; AN INTERNATIONAL JOURNAL ON MICRO AND TRACEANALYSIS, SPRINGER-VERLAG, VI, vol. 168, no. 1-2, 12 December 2009 (2009-12-12), pages 87-92, XP019782925, ISSN: 1436-5073	1,2,4-8, 11,12, 15-20
Y	abstract pages 88-89	3,9,10, 13,14
	----- -/--	

[X] Further documents are listed in the continuation of Box C. [ ] See patent family annex.

* Special categories of cited documents :

"A" document defining the general state of the art which is not considered to be of particular relevance

"E" earlier document but published on or after the international filing date

"L" document which may throw doubts on priority claim(s) or which is cited to establish the publication date of another citation or other special reason (as specified)

"O" document referring to an oral disclosure, use, exhibition or other means

"P" document published prior to the international filing date but later than the priority date claimed

"T" later document published after the international filing date or priority date and not in conflict with the application but cited to understand the principle or theory underlying the invention

"X" document of particular relevance; the claimed invention cannot be considered novel or cannot be considered to involve an inventive step when the document is taken alone

"Y" document of particular relevance; the claimed invention cannot be considered to involve an inventive step when the document is combined with one or more other such documents, such combination being obvious to a person skilled in the art.

"&" document member of the same patent family

Date of the actual completion of the international search	Date of mailing of the international search report
8 November 2011	21/11/2011

Name and mailing address of the ISA/	Authorized officer
European Patent Office, P.B. 5818 Patentlaan 2 NL - 2280 HV Rijswijk Tel. (+31-70) 340-2040, Fax: (+31-70) 340-3016	Michalitsch, Richard

INTERNATIONAL SEARCH REPORT

International application No
PCT/US2011/046214

C(Continuation). DOCUMENTS CONSIDERED TO BE RELEVANT

Category*	Citation of document, with indication, where appropriate, of the relevant passages	Relevant to claim No.
X,P	DING YU ET AL: "Electrospun Co3O4 nanofibers for sensitive and selective glucose detection.", BIOSENSORS & BIOELECTRONICS 15 OCT 2010 LNKD- PUBMED:20810272, vol. 26, no. 2, 15 October 2010 (2010-10-15), pages 542-548, XP002662987, ISSN: 1873-4235 the whole document	1-20
X	WANG W ET AL: "Electrospun palladium (IV)-doped copper oxide composite nanofibers for non-enzymatic glucose sensors", ELECTROCHEMISTRY COMMUNICATIONS, ELSEVIER, AMSTERDAM, NL, vol. 11, no. 9, 1 September 2009 (2009-09-01), pages 1811-1814, XP026716408, ISSN: 1388-2481, DOI: 10.1016/J.ELECOM.2009.07.025 [retrieved on 2009-07-30]	1,2,4-8, 11,12, 15-20
Y	abstract page 1812 - page 1813	3,9,10, 13,14
X	LU L M ET AL: "A nano-Ni based ultrasensitive nonenzymatic electrochemical sensor for glucose: Enhancing sensitivity through a nanowire array strategy", BIOSENSORS AND BIOELECTRONICS, ELSEVIER BV, NL, vol. 25, no. 1, 15 September 2009 (2009-09-15), pages 218-223, XP026438608, ISSN: 0956-5663 [retrieved on 2009-07-07]	1,2,4-8, 11,12, 15-20
Y	the whole document	3,9,10, 13,14